2014

Crustal Shortening, Exhumation, and Strain Localization in a Collisonal Orogen: the Bajo Pequeno Shear Zone, Sierra de Pie de Palo, Argentina

Joshua M. Garber

Sarah M. Roeske

Jessica Warren

Sean R. Mulcahy
Western Washington University, sean.mulcahy@wwu.edu

William C. McClelland

See next page for additional authors

Recommended Citation

Garber, J. M., S. M. Roeske, J. Warren, S. R. Mulcahy, W. C. McClelland, L. J. Austin, P. R. Renne, and G. I. Vujovich (2014), Crustal shortening, exhumation, and strain localization in a collisional orogen: The Bajo Pequeño Shear Zone, Sierra de Pie de Palo, Argentina, Tectonics, 33, 1277–1303, doi:10.1002/2013TC003477

Authors
Joshua M. Garber, Sarah M. Roeske, Jessica Warren, Sean R. Mulcahy, William C. McClelland, Lauren J. Austin, Paul R. Renne, and Graciela I. Vujovich

AGU PUBLICATIONS

Tectonics

RESEARCH ARTICLE
10.1002/2013TC003477

Key Points:
- BPSZ deformation is associated with the establishment of a new plate boundary
- Strain localization in the BPSZ overprints an early inverted thermal gradient
- Structures in the Famatinian system show strain localization over ~70 Myr

Supporting Information:
- Readme
- Table S1
- Table S2
- Table S3

Correspondence to:
J. M. Garber,
jmgarber@umail.ucsb.edu

Citation:
Garber, J. M., S. M. Roeske, J. Warren, S. R. Mulcahy, W. C. McClelland, L. J. Austin, P. R. Renne, and G. I. Vujovich (2014), Crustal shortening, exhumation, and strain localization in a collisional orogen: The Bajo Pequeño Shear Zone, Sierra de Pie de Palo, Argentina, *Tectonics*, *33*, 1277–1303, doi:10.1002/2013TC003477.

Received 11 NOV 2013
Accepted 22 MAY 2014
Accepted article online 5 JUN 2014
Published online 7 JUL 2014

Crustal shortening, exhumation, and strain localization in a collisional orogen: The Bajo Pequeño Shear Zone, Sierra de Pie de Palo, Argentina

Joshua M. Garber[1,2], Sarah M. Roeske[1], Jessica Warren[3], Sean R. Mulcahy[4], William C. McClelland[5], Lauren J. Austin[6], Paul R. Renne[4,7], and Graciela I. Vujovich[8,9]

[1]Department of Geology, University of California, Davis, California, USA, [2]Now at Department of Earth Science, University of California, Santa Barbara, California, USA, [3]Department of Geological and Environmental Sciences, Stanford University, Stanford, California, USA, [4]Department of Earth and Planetary Science, University of California, Berkeley, California, USA, [5]Department of Geoscience, University of Iowa, Iowa City, Iowa, USA, [6]Department of Geological Sciences, University of Oregon, Eugene, Oregon, USA, [7]Berkeley Geochronology Center, Berkeley, California, USA, [8]CONICET, Buenos Aires, Argentina, [9]Laboratorio de Tectonica Andina-FCEyN, Universidad de Buenos Aires, Buenos Aires, Argentina

Abstract The Bajo Pequeño Shear Zone (BPSZ) is a lower-crustal shear zone that records shortening and exhumation associated with the establishment of a new plate boundary, and its placement in a regional structural context suggests that local- to regional-scale strain localization occurred with progressive deformation. A kilometer-scale field and analytical cross section through the ~80 m thick BPSZ and its adjacent rocks indicates an early Devonian (405–400 Ma) phase of deformation on the western margin of Gondwanan continental crust. The earliest stages of the BPSZ, recorded by metamorphic and microstructural data, involved thrusting of a hotter orthogneiss over a relatively cool pelitic unit, which resulted in footwall garnet growth and reset footwall white mica $^{40}Ar/^{39}Ar$ ages in proximity to the shear zone. Later stages of BPSZ activity, as recorded by additional microstructures and quartz *c*-axis opening angles, were characterized by strain localization to the center of the shear zone coincident with cooling and exhumation. These and other data suggest that significant regional tectonism persisted in the Famatinian orogenic system for 60–70 million years after one microplate collision (the Precordillera) but ceased 5–10 million years prior to another (Chilenia). A survey of other synchronous structures shows that strain was accommodated on progressively narrower structures with time, indicating a regional pattern of strain localization and broad thermal relaxation as the Precordillera collision evolved.

1. Introduction

The exhumed roots of collisional orogens allow geologists to examine the accommodation of strain in continental crust, particularly how strain evolves with progressive deformation or changes in geodynamic boundary conditions, such as the cessation or reestablishment of subduction. Units or blocks involved in these collisions can preserve complex tectonic histories spanning multiple orogenies, and often record time- or space-limited deformation events. A full understanding of convergent margin history requires detailed field, structural, petrologic, geochronological and thermochronological analyses of individual structures, coupled with the integration of regional data. Together, these data sets can shed light on when, where, and how strain is accommodated in convergent settings.

Collisional orogens also provide a means to study the driving factors behind strain localization, and the time scales over which localization can occur. Field evidence from exhumed lower- and mid-crustal metamorphic rocks shows that strain localization is ubiquitous in the deep crust [e.g., *Simpson et al.*, 2001; *White*, 2004; *Williams et al.*, 2009], suggesting that the principal driver behind ductile strain localization relates to non-uniform rock strength, either between different lithologies [e.g., *Waters-Tormey and Tikoff*, 2007] or between shear zones and their adjacent rocks [e.g., *Rutter et al.*, 2001]. Many of these studies have focused on shear zone reactivation [e.g., *Simpson et al.*, 2001], in which the initial high-temperature deformation that produced the high-strain zone is separated by millions to billions of years from later, cooler deformation that exploited the preexisting weakness in the rock. The processes that govern strain localization during individual deformation

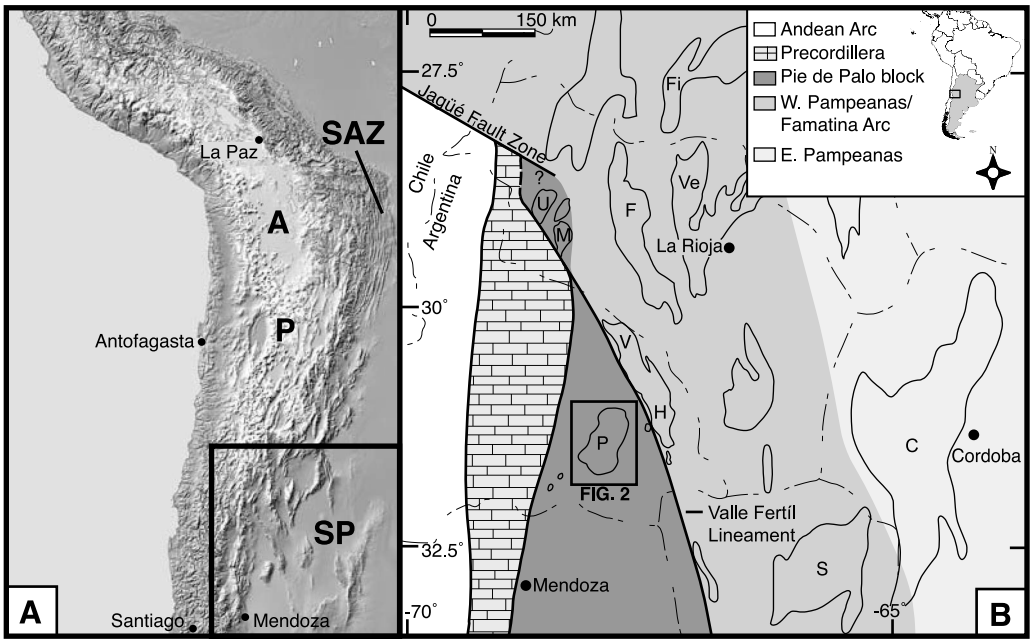

Figure 1. Regional geology of the central Andean margin and the Sierras Pampeanas. (a) Shaded relief map of western South America illustrating the geographic location of the Bolivian Subandean Zone (SAZ), the Altiplano (A), the Puna (P), and the Sierras Pampeanas (SP). (b) Tectonic map of boxed area in Figure 1a. Individual ranges are outlined, as are terrane boundaries (bold) and country/province boundaries (thin lines). Ranges shown include the Sierras de Cordoba (C), de Famatina (F), de Fiambala (Fi), de la Huerta (H), de Maz (M), de Pie de Palo (P), de San Luis (S), de Umango (U), de Valle Fertil (V), and de Velasco (Ve). Topographic contours were extracted from the 30 m resolution ASTER global digital elevation model (a product of METI and NASA). Figure modified from *Mulcahy et al.* [2011].

events or orogenic cycles are less clear. This is especially important because changes in the localization of strain can have a profound influence on the strength of the entire lithosphere [e.g., *Burgmann and Dresen*, 2008; *Platt and Behr*, 2011b]. Because deeply exhumed collisional margins preserve structures that were active at different times and under evolving conditions during progressive deformation, they provide a unique opportunity to identify the root causes of strain localization and to clarify the timing of this localization.

The basement uplifts of the Western Sierras Pampeanas of west central Argentina (Figure 1) expose a Late Precambrian to mid-Paleozoic convergent to collisional margin, affording the opportunity to document how different levels of the crust accommodated and recorded strain during the evolution of this margin. Many of the rocks were deformed initially during the Mesoproterozoic assembly of Rodinia [e.g., *Casquet et al.*, 2012], rifted apart during the Neoproterozoic [e.g., *Baldo et al.,* 2006], and deformed again during an Ordovician microplate collision along the western margin of Gondwana [*Casquet et al.,* 2001; *Vujovich et al.,* 2004; *van Staal et al.,* 2011; *Mulcahy et al.*, 2014]. Recent work in the Sierra de Pie de Palo (Figure 2), located within the forearc of the Ordovician event, suggests an extended period of deformation from ~515–400 Ma associated with numerous west-verging structures that accommodated the collision [*Ramos et al.*, 1998; *Mulcahy et al.*, 2007, 2011]. Previous work has generally focused on the west and east sides of the Pie de Palo, but sparse and conflicting data from the poorly-accessible Central Complex (section 2.1, below), which makes up nearly two thirds of the range, limits the scale of tectonic interpretations.

Here we present data from a lower to mid-crustal retrograde ductile shear zone, the Bajo Pequeño Shear Zone (BPSZ; Figures 3 and 4), from the Central Complex of the Pie de Palo. These data include field traverses and structural measurements, thermobarometry, quartz microstructural analyses, $^{40}Ar/^{39}Ar$ thermochronology, and U-Pb zircon geochronology; the combination of these complementary data allows an integrated approach to studying the shear zone. Analysis of the different stages of metamorphism and deformation recorded by the shear zone and the units it separates indicates that the shear zone is a significant structure that initially formed under lower-crustal *P-T* conditions and juxtaposed rocks with distinct detrital, structural, and metamorphic histories. Furthermore, each data set reported here preserves a portion of the full evolution of

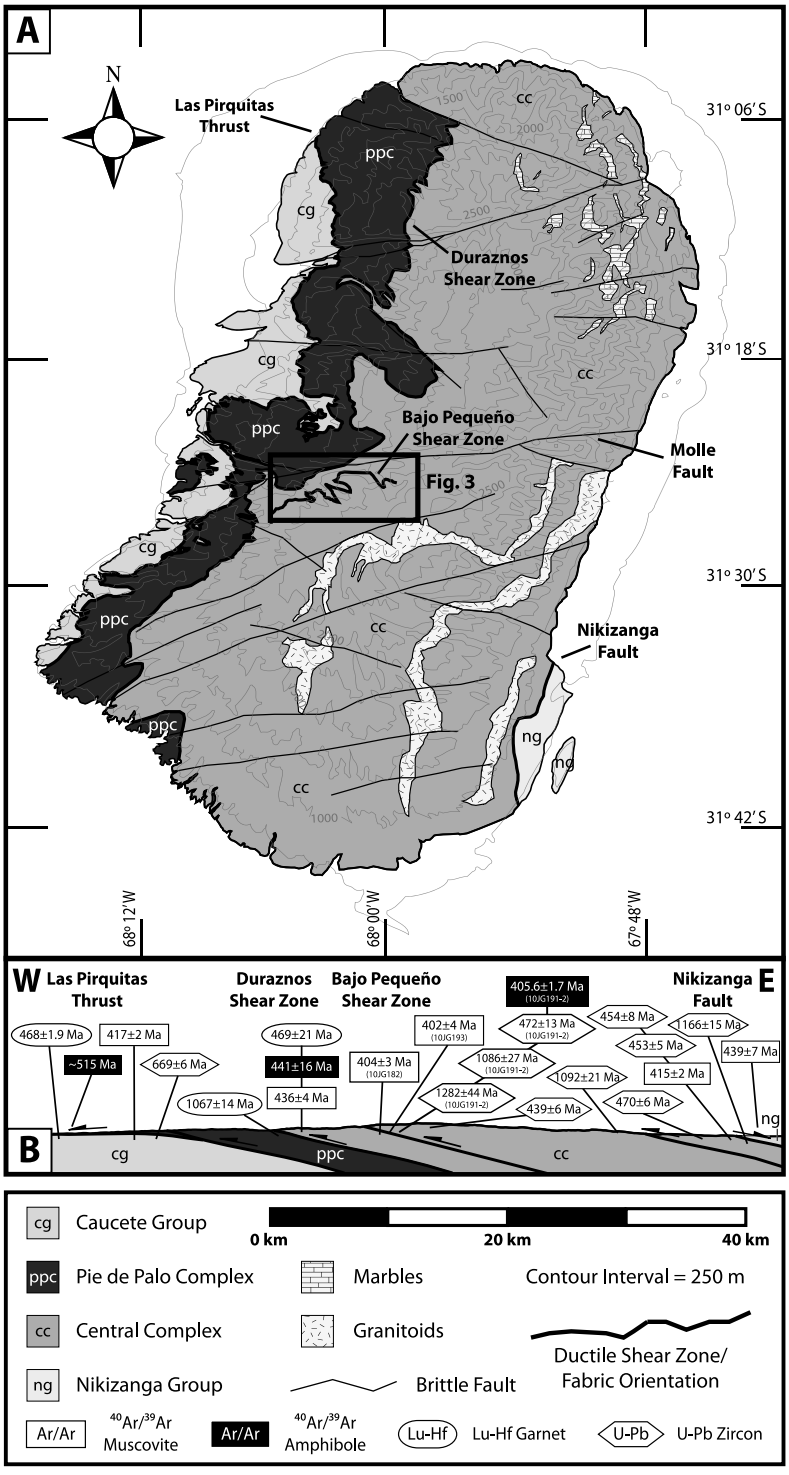

Figure 2. Geologic map and cross section of the Sierra de Pie de Palo. (a) Geologic map of the Pie de Palo showing first-order structures and lithologies within the range; the black box outlines the more detailed geologic map shown in Figure 3. The map was compiled from regional mapping, published maps [*Ramos and Vujovich*, 2000; *Mulcahy et al.*, 2011, and references therein], and our observations from multispectral ASTER satellite data. The southern part of the Pie de Palo includes speculative ductile shear zones and foliation markers; both were identified in ASTER data and help constrain the general structure of the range. (b) Schematic cross section of the Pie de Palo, roughly to scale, shown along a general E-W transect; the cross section is interpretive at depth. Lu-Hf garnet ages are from *Mulcahy et al.* [2011], and U-Pb zircon and $^{40}Ar/^{39}Ar$ hornblende and muscovite ages are from *Mulcahy et al.* [2007, 2011] and this study (the latter marked with an asterisk). Samples from this study are shown with their sample number. The cross section is modified from *Mulcahy et al.* [2011].

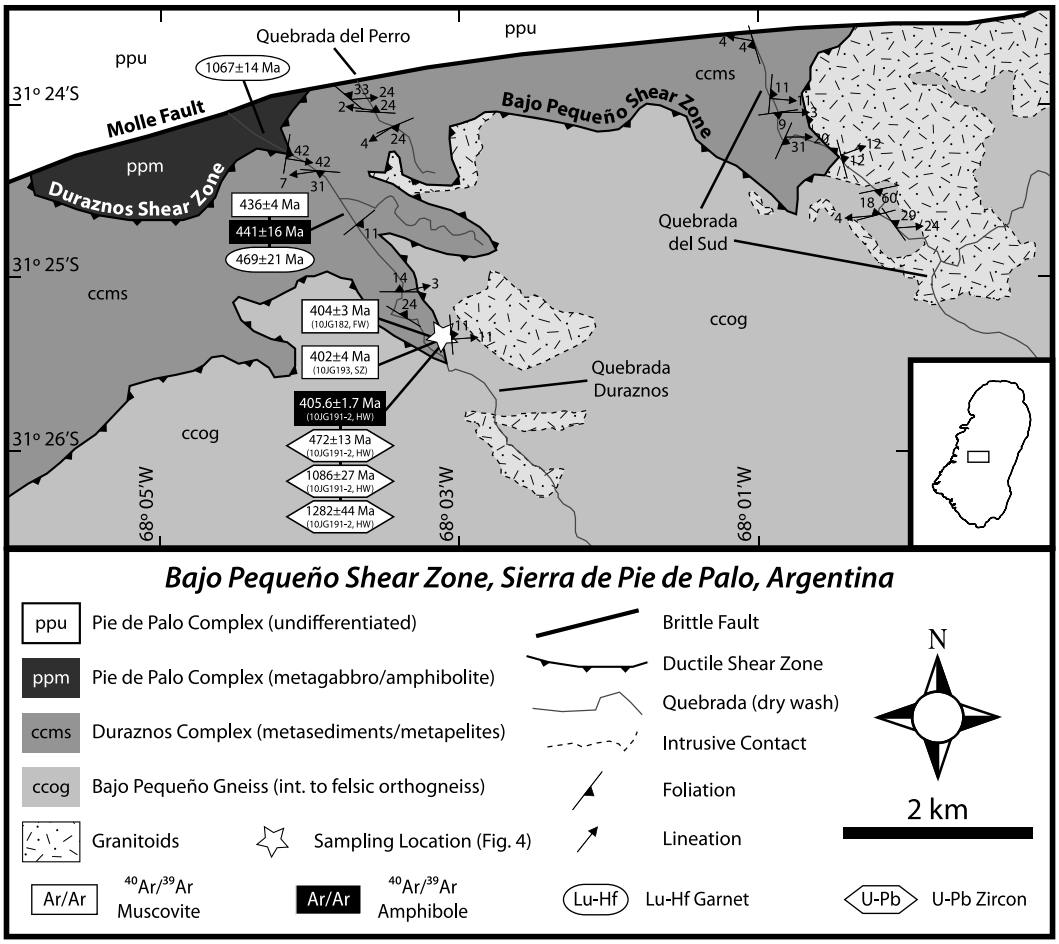

Figure 3. Geologic map of the Bajo Pequeño Shear Zone. Geologic map of the BPSZ based on field observations in Quebradas Duraznos, del Perro, and Sud; observations from ASTER images were used to extend boundaries and contacts between washes. The inset outline of the Pie de Palo indicates the location of the map relative to the rest of the range. The Duraznos Shear Zone, investigated by *Mulcahy et al.* [2011], represents the lower structural boundary of the Central Complex with the mafic-ultramafic Pie de Palo Complex. The location of the cross section (Figure 4) and all samples is marked by a white star. Relevant ages from *Mulcahy et al.* [2011] and this study are indicated at their sampling locations; because samples from the BPSZ were all collected at the location of the white star, their sample numbers and affinity (FW, SZ, and HW) are included for reference. Granitoids similar to those shown on the map have protolith ages of ~938 to ~1091 Ma [*McDonough et al.*, 1993], but their exact sampling location and their relationship to the Bajo Pequeño Gneiss are not known. Foliation and lineation data include multiple structural generations.

the shear zone: metamorphic *P-T* conditions, metamorphic fabrics, and quartz slip systems indicate that the earliest stages of deformation were characterized by overthrusting of a hotter hanging wall and localized metamorphism in the footwall. Quartz *c*-axis opening angles, recrystallization textures, and thermochronology data suggest that progressive localization of strain to the center of the shear zone occurred during exhumation, as deformation temperature fell and strain rate increased.

Our coeval hornblende and muscovite thermochronology documents that rapid cooling occurred along the shear zone during the early Devonian (405–400 Ma), which we attribute to rapid exhumation after localized shortening and metamorphism. These results also indicate that the footwall rocks to the shear zone experienced renewed tectonic burial after partial exhumation at 440–435 Ma. The recognition of this mid-Paleozoic activity tied to a specific exhumational structure confirms earlier work [*Ramos et al.*, 1998] identifying this time period as the latest phase of Paleozoic tectonism in the Pie de Palo. Finally, the synchronous timing and style of deformation along the BPSZ and other regional structures suggests regional-scale strain localization with time, from penetrative metamorphism and deformation (470–465 Ma) to exhumation along kilometer-scale (440–435 Ma) and hectometer-scale (405–395 Ma) ductile shear zones.

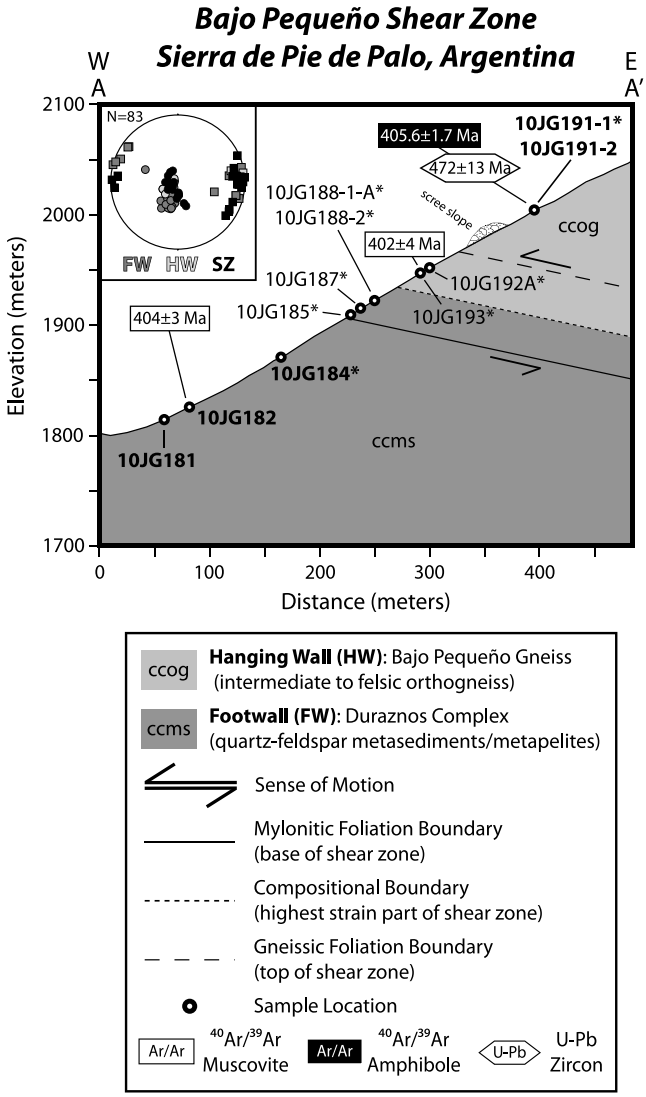

Figure 4. Geologic cross section of the BPSZ, at the location marked by the white star in Figure 3. The top-to-the-west, thrust-sense shear zone separates footwall Duraznos Complex metasediments from hanging wall Bajo Pequeño Gneiss. The upper and lower boundaries of the shear zone, as well as the compositional boundary in the center of the shear zone, are shown here; see text for discussion of their placement. Structural data from the footwall, hanging wall, and shear zone are shown in the inset stereoplot with a different gray scale for each. Circles are poles to foliation and squares are lineations. These data show a shallowly east-dipping foliation with variable strike and a consistent E-W stretching lineation. Samples analyzed in this study are shown by black circles: samples in bold text were used to calculate metamorphic *P-T* conditions, and those marked by an asterisk were analyzed for quartz *c*-axis fabrics. Selected $^{40}Ar/^{39}Ar$ and U-Pb ages from this study are shown; Precambrian U-Pb ages from the hanging wall are excluded for clarity.

2. Geology of the Western Sierras Pampeanas and the Sierra de Pie de Palo

The Sierras Pampeanas of NW Argentina consist of basement-cored uplifts exposed during the Late Miocene to recent Andean orogeny, separated by generally undeformed sedimentary basins [*Allmendinger et al.,* 1990*; Zapata,* 1998*; Gimenez et al.,* 2000*; Ramos et al.,* 2002*; Alvarado et al.,* 2005] (Figure 1). In particular, the lower to mid-crustal rocks of the Western Sierras Pampeanas record an extended period of deformation that occurred on the Late Precambrian to mid-Paleozoic Gondwanan margin. One phase of this deformation, the Famatinian orogeny [e.g., *Ramos et al.,* 1998], has been ascribed to the subduction and collision of the allochthonous, Laurentian-derived Precordillera terrane from ~500–400 Ma. Peak metamorphic conditions and a top-to-the-west penetrative deformation event associated with the collision are recognized across the Famatinian margin at ~470–460 Ma [*Ramos et al.,* 1998*; Casquet et al.,* 2001*; Vujovich et al.,* 2004*; Mulcahy et al.,* 2011].

Located between the Precordillera (to the west) and the Famatinian magmatic arc (to the east) (Figure 1), the Sierra de Pie de Palo (herein referred to as the Pie de Palo; Figure 2a) preserves an imbricate series of granulite to greenschist facies metamorphic units situated in the forearc of the Famatinian collisional zone. These rocks record a >100 Ma record of the Famatinian orogeny, from ~515 Ma ductile thrusting [*Mulcahy et al.,* 2007] to ~400 Ma exhumation and late cooling [*Ramos et al.,* 1998*;* this work]. The western two thirds of the range records top-to-the-west thrusting along ductile shear zones but the easternmost part of the range records a top-to-the-east, normal-sense shear zone that juxtaposes upper- and lower-crustal units [e.g., *Mulcahy et al.,* 2011] (Figure 2b). Activity along these opposing-sense shear zones was at least partly coeval, suggesting synconvergent extension and exhumation at 440–435 Ma [*Mulcahy et al.,* 2011].

2.1. The Central Complex of the Pie de Palo

Previous workers [e.g., *Mulcahy et al.,* 2011] have recognized four distinct lithotectonic packages within the Sierra de Pie de Palo based on lithology, metamorphic grade, and major unit-bounding shear zones.

From west to east these are the *Caucete Group* (metasedimentary and metavolcanic), *Pie de Palo Complex* (mafic-ultramafic), *Central Complex* (mixed metasedimentary and metaigneous), and *Nikizanga Group* (low- to medium-grade metasediments) (Figure 2). As the focus of this study is on the Central Complex, we briefly discuss previous work on this unit.

Excluding the Nikizanga Group, various authors have designated the eastern two thirds of the range as the Central Complex [*Ramos et al.*, 1998; *Ramos and Vujovich*, 2000; *Mulcahy et al.*, 2011]. Following *Mulcahy et al.* [2011], we use this term broadly to refer to all of the rock units located between the Duraznos and Nikizanga shear zones, which includes metasediment, metapelite, carbonate, metavolcanics, amphibolite, orthogneiss, quartzite, and migmatite, including the subdivisions of *Casquet et al.* [2001], *Galindo et al.* [2004], and *Baldo et al.* [2006]. These and other studies have reported Mesoproterozoic to mid-Paleozoic igneous, metamorphic, and cooling ages from across the complex, in addition to variable peak metamorphic conditions from different locations [*Ramos et al.*, 1998; *Baldo et al.*, 2006; *Rapela et al.*, 2010; *Mulcahy et al.*, 2011]. *Casquet et al.* [2001], in their analysis of an outcrop near the Molle fault, noted Ordovician (~465 Ma) metamorphism along a clockwise *P-T* trajectory. This metamorphic event culminated in peak conditions of 13 ± 1 kbar and 600 ± 50°C followed by decompression during ductile deformation to 9.0 ± 1.3 kbar and 570 ± 5°C. Rocks from the structurally lowest section of the Central Complex, in the hanging wall of the Duraznos Shear Zone, exhibit similar metamorphic ages (~470 Ma) and *P-T* conditions (9.3 ± 0.8 kbar, 638 ± 15°C) [*Mulcahy et al.*, 2011] (Figure 3). However, rocks from the structurally highest section of the Central Complex record much higher-grade conditions (13.9 ± 1.4 kbar, 734 ± 37°C) [*Mulcahy et al.*, 2011].

The deformation history of the Central Complex during the latest stages of the Famatinian collision is as yet unclear. *Mulcahy et al.* [2011] reported coeval, Silurian (440–435 Ma) $^{40}Ar/^{39}Ar$ muscovite cooling ages on the two shear zones that bound the Central Complex (Figure 2b). This geometry suggests that the Central Complex could have exhumed as a coherent wedge with little internal deformation by ~435 Ma, which is supported by other data suggesting that peak metamorphism ended prior to this time [e.g., *Casquet et al.*, 2001]. However, scattered late cooling ages from the Central Complex (412.7 ± 0.3 Ma, 394.3 ± 0.2 Ma) [*Ramos et al.*, 1998] and significant changes in metamorphic grade and histories across the complex [*Mulcahy et al.*, 2011] strongly suggest the presence of additional *P-T* breaks (i.e., shear zones) across the range.

2.2. First-Order Ductile Structures in the Pie de Palo

Previous work focused on the ductile structures that separate the major lithologic packages of the Pie de Palo (Figure 2). Note that Miocene to recent brittle deformation has offset these ductile structures along major faults or "megafractures" [*Zapata*, 1998], such as the east-west trending El Molle fault in the center of the range (e.g., Figure 3).

The shallowly east-dipping, top-to-the-west Las Pirquitas Thrust (LPT) places the Pie de Palo Complex in the hanging wall over the Caucete Group in the footwall. This thrust is marked by a meter-scale retrograde shear zone that overprints and deforms an older, higher-temperature, multiply-folded mylonitic fabric [*Mulcahy et al.*, 2007, 2011; *van Staal et al.*, 2011]. *Mulcahy et al.* [2007] reported 515 ± 2 and 510 ± 3 Ma $^{40}Ar/^{39}Ar$ hornblende crystallization ages from the immediate hanging wall of the Las Pirquitas Thrust, in the higher-temperature fabric that was redeformed at cooler temperatures. A Lu-Hf garnet age from the footwall of the thrust records peak metamorphism in the Caucete Group at 468 ± 2 Ma [*Mulcahy et al.*, 2011], similar to a $^{40}Ar/^{39}Ar$ hornblende age of 464.3 ± 0.3 Ma near the fault zone but ~20 km to the south [*Ramos et al.*, 1998]. Cooling events in the footwall are constrained by $^{40}Ar/^{39}Ar$ muscovite ages of 417 ± 2 Ma [*Mulcahy et al.*, 2011] and 395.7 ± 0.2 Ma [*Ramos et al.*, 1998]. These ages, coupled with detailed structural analyses [*van Staal et al.*, 2011], suggest that the Las Pirquitas Thrust is a long-lived structure that experienced episodic reactivation.

The southeast-dipping, oblique top-to-the-west Duraznos Shear Zone separates mafic and ultramafic intrusives and metavolcanics of the Pie de Palo Complex in the footwall from the metasedimentary base of the Central Complex in the hanging wall (Figure 3). The shear zone was investigated by *Mulcahy et al.* [2011], who reported a ~600 m wide mylonite zone in the central part of the range. Prekinematic Lu-Hf garnet core ages from hanging wall Central Complex metapelites record metamorphism at 469 ± 21 Ma, and $^{40}Ar/^{39}Ar$ synkinematic hornblende and muscovite ages from the hanging wall record cooling at 441 ± 16 and 436 ± 4 Ma, respectively [*Mulcahy et al.*, 2011]. These ages were interpreted to suggest penetrative deformation and metamorphism starting with the Ordovician collision of the Precordillera and culminating with exhumation to the middle crust 25–30 Ma later [*Mulcahy et al.*, 2011].

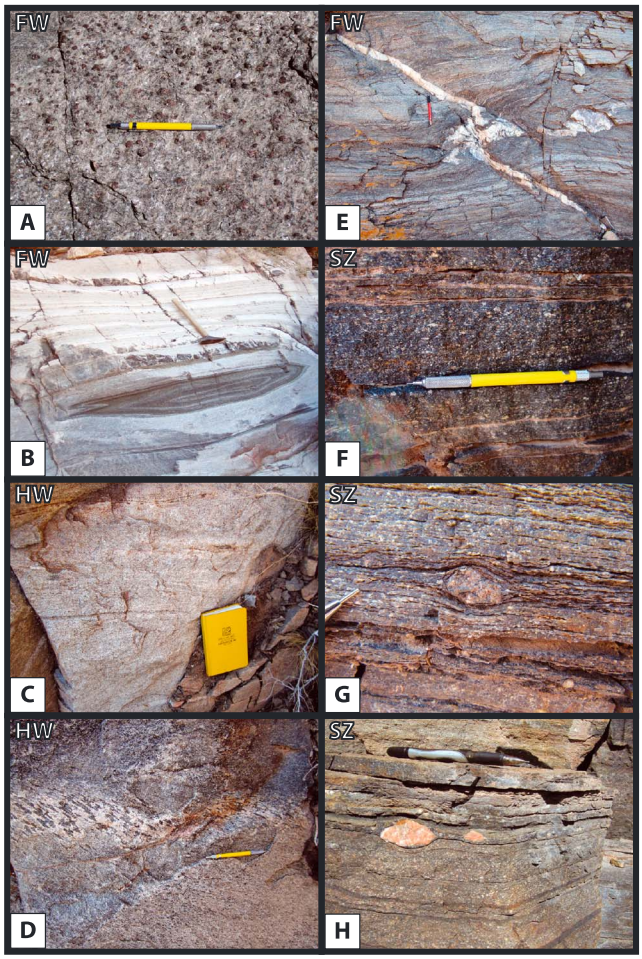

Figure 5. Outcrop Photos of the Bajo Pequeño Shear Zone, labeled as footwall (FW), hanging wall (HW), or shear zone (SZ). (a) Garnet-bearing metapelitic schists in the Duraznos Complex. In some locations the garnet porphyroblasts approach 2–3 cm in size. (b) Quartzo-feldspathic metasediments (Duraznos Complex) exhibiting compositional banding. The structure at the base of the photograph may be a sheath fold. (c) Felsic, quartzo-feldspathic orthogneiss in the hanging wall Bajo Pequeño Gneiss. The gneissic fabric is either related to Grenville deformation at ~1.07 Ga or high-*T* deformation at ~470 Ma. (d) Mafic clasts in a quartzo-feldspathic matrix that indicate a top-to-the-west shear sense for the hanging wall Bajo Pequeño Gneiss. This high-*T* fabric was likely acquired at the same time as the gneissic foliation. (e) Quartz vein oriented ~45° from the foliation plane, <100 m below the shear zone. (f) Flattened, platy shear zone mylonite with numerous plagioclase (light colored) and garnet (red) porphyroclasts. (g) Sigma-type (asymmetric) feldspar porphyroclast from near the base of the shear zone; the stair-stepping tails on the outer edge of the clast indicate a top-to-the-west shear sense (sinistral in this photo). (h) Millimeter to centimeter-scale, theta-type (symmetric) feldspar porphyroclasts with no clear shear sense, in the upper part of the shear zone.

The east-dipping, top-to-the-east Nikizanga Fault places low-grade metasediments of the Nikizanga Group against the high-grade rocks of the Central Complex [e.g., *Mulcahy et al.*, 2011]. A $^{40}Ar/^{39}Ar$ muscovite cooling age from the hanging wall (439 ± 6 Ma) suggests extension on the Nikizanga Fault coeval with thrusting along the Duraznos Shear Zone at 440–435 Ma [*Mulcahy et al.*, 2011].

3. Field Observations of the Lower Central Complex

What follows is a description of the lithologic units that we observed at the structurally deepest levels of the Central Complex, including a description of the Bajo Pequeño Shear Zone.

3.1. Duraznos Complex and Bajo Pequeño Gneiss

In the Quebrada Duraznos area, south of the Molle fault, we delineate two units overlying the Duraznos Shear Zone. The lowermost unit, in the immediate hanging wall to the Duraznos Shear Zone and also described by *Mulcahy et al.* [2011], is termed the "Duraznos Complex" (Figures 3 and 4). This unit consists of garnet-bearing pelitic schists (Figure 5a), quartzo-feldspathic metasediments (Figure 5b), intermediate to felsic orthogneiss, and rare green amphibolite pods. The felsic orthogneiss is restricted to a narrow 0.5 km band in the immediate hanging wall of the Duraznos Shear Zone; the upper part of the Duraznos Complex lacks this orthogneiss but includes the addition of rare amphibole-clinozoisite gneiss and quartzite. In addition to the *P-T*, Lu-Hf, and $^{40}Ar/^{39}Ar$ data reported previously for this unit by *Mulcahy et al.* [2011] and discussed above, *Austin et al.* [2011] reported a maximum depositional age of 966 ± 36 Ma for the Duraznos Complex.

The Duraznos Complex is crosscut by the Bajo Pequeño Shear Zone (Figures 3 and 4) and overlain by the Bajo Pequeño Gneiss, a massive quartzo-feldspathic orthogneiss (Figure 5c). Within the Bajo Pequeño Gneiss, leucocratic stringers are present, as are biotite-rich mafic enclaves (Figure 5d), restitic pods, and sparse mica-rich layers. Previous U-Pb zircon analyses show that this unit crystallized at ~1245 Ma, and zircons have igneous zoning in their cores with metamorphic rims [*Austin et al.*, 2011].

3.2. Structure: Bajo Pequeño Shear Zone

The main exposure of the BPSZ was investigated in a small drainage (i.e., Bajo Pequeño) off the main part of Quebrada Duraznos. It was traced over a larger extent by combining lithologic and structural data from a similar sequence exposed in Quebrada del Sud, where the high-strain zone itself is covered, with Advanced Spaceborne Thermal Emission and Reflection (ASTER) multispectral satellite imagery (Figure 3). As previously noted, the BPSZ separates the footwall Duraznos Complex from the overlying Bajo Pequeño Gneiss. Outcrops of the shear zone are limited, but where present, exposure is excellent. All foliations (footwall, shear zone, and hanging wall) are shallowly east-dipping and the principal stretching lineation is oriented E-W (Figure 4).

The footwall schistose foliation becomes more parallel and increasingly penetrative approaching the shear zone, with grain size reduction present in metapelitic outcrops tens of meters below the shear zone. Rare quartz veins are oriented in the shear plane at a ~45° angle to the foliation (Figure 5e). A few meters below the shear zone, the foliation tilts to near-vertical and rotates westward into a platy mylonite that defines the edge of the high-strain zone. This mylonite has a black matrix with light-colored, millimeter- to centimeter-scale porphyroclasts (Figure 5f). Mixing of the hanging wall and footwall lithologies occurs among the mylonites but a rough lithologic boundary is inferred between outcrops of dominantly metapelitic and metaigneous affinity. Fabric intensity increases toward the center of the shear zone as the grain size decreases. Additionally, a transition occurs from asymmetric, top-to-the-west, σ-type porphyroclasts at the base of the shear zone (Figure 5g) to symmetric, φ- and θ-type porphyroclasts at its upper edges (Figure 5h).

Continuing upsection into the hanging wall, the grain size increases, a gneissic fabric is developed, and shear sense indicators return to a dominant top-to-the-west orientation. Samples (10JG181–10JG193) of metapelitic and metaigneous schists, gneisses, and mylonites were collected at intervals below, within, and above the shear zone (Figure 4). The structurally highest samples were collected from micaceous (10JG191-1) and quartzo-feldspathic (10JG191-2) sections of orthogneiss that exhibits gneissic banding at outcrop scale. Access farther upsection of these two samples was not possible. The gneissic banding, as well as boudins of mafic or tonalitic material, is recognized starting just upsection of sample 10JG192A/B, where a transition to lower strain is clear. However, a strong S-C fabric is observed in these highest samples, with deformed porphyroclasts that indicate protomylonitic to mylonitic deformation conditions. It is therefore unclear how far deformation related to shear zone activity propagated into the orthogneiss. For consistency, we mark the upper boundary of the shear zone at the transition to a recognizable gneissic foliation in the hanging wall, such that both shear zone boundaries are placed at significant fabric (and therefore strain) transitions. Using these boundaries, the estimated thickness of the shear zone in this location is 80 ± 10 m (Figure 4).

4. Petrology and Thermobarometry

Samples collected from the footwall and the hanging wall of the BPSZ were used to determine their metamorphic histories and *P-T* conditions, and to constrain any pressure or temperature gradients or breaks.

4.1. Methods

Mineral compositions were determined by electron probe microanalysis (EPMA) on a Cameca SX-100 at UC-Davis. Natural and synthetic mineral samples were used as standards. An accelerating voltage of 15 kV was used for all analyses, with a 1 μm beam for garnet, amphibole, and staurolite, a 5 μm beam for biotite and epidote, and a 10 μm beam for white mica, plagioclase, and K-feldspar. All garnet X-ray maps (e.g., Figure 6) utilized the same accelerating voltage with an 80 nA beam current, a beam size of 1 μm, and variable step sizes between 1 and 4 μm. The location of quantitative garnet traverses were selected after X-ray maps were completed. End-member garnet components were calculated using the Excel spreadsheet of *Locock* [2008] and are reported as spessartine [Sps], almandine [Alm], pyrope [Prp], and grossular [Grs]. Pressure and temperature conditions were estimated by the avPT method [*Powell and Holland*, 1994] using the software THERMOCALC (v3.33), with the updated data set of *Holland and Powell* [1998]. Microprobe analyses used for thermobarometry are contained in the supporting information. Mineral activities and ferric iron were calculated with the software AX (version 0.3). All quantitative mineral analyses are from porphyroblast rims and adjacent or nearby matrix minerals; all THERMOCALC analyses include the addition of pure H_2O. Table 1 contains a summary of all THERMOCALC data.

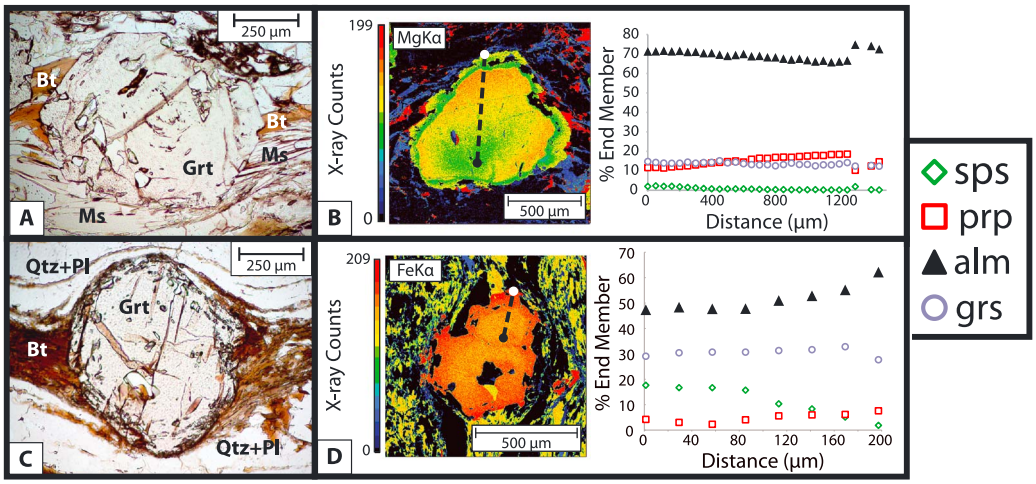

Figure 6. Petrographic textures and X-Ray maps of metamorphic garnet. (a) Plane-polarized light (PPL) thin section image of two-stage metamorphic garnet from sample 10JG181 (footwall); the textures suggest both prekinematic and postkinematic metamorphic mineral growth (see text for discussion). (b) Magnesium X-ray map and microprobe traverse of a two-stage metamorphic garnet from sample 10JG181, showing two prograde paths separated by a resorption surface. (c) PPL thin section image of metamorphic garnet from sample 10JG191-1 (hanging wall). This garnet records a single phase of growth and is wrapped by the foliation. (d) Iron X-ray map and microprobe traverse of a single-stage metamorphic garnet from sample 10JG191-1, showing a single prograde path. Run conditions for X-ray maps and chemical traverses in Figures 6b and 6d are discussed in the text. The color scales for X-ray maps are based on absolute microprobe counts; black circles mark the start of each traverse, and white circles mark their end points.

4.2. Results: *P-T*

4.2.1. Footwall

The structurally lowest sample collected from the BPSZ (sample 10JG181) is a Grt-St-Ky-Bt-Ms-Qtz-Pl pelitic schist from the footwall Duraznos Complex (mineral abbreviations after *Kretz* [1983]). Two garnet morphologies are present in the sample: a coarse-grained (1–2 mm), poikiloblastic variety with euhedral overgrowths (Figures 6a and 6b), and a finer-grained (<1 mm) euhedral, inclusion-poor variety. Coarse garnet cores appear to deflect the penetrative schistosity and record an older fabric at an angle to the external foliation, but rim overgrowths and finer garnets overprint the foliation (Figure 6a). X-ray chemical zoning patterns for the coarse garnet indicate two prograde core-to-rim transitions (decreasing Sps, Alm, and increasing Prp), separated by an uneven resorption surface (Figure 6b). The fine-grained garnets preserve only a single prograde path that is compositionally similar to the coarse-grained garnet rims. These relationships suggest a major phase of prekinematic garnet growth followed by later postkinematic growth, likely reflecting two distinct metamorphic events. Staurolite and kyanite are also porphyroblastic but lack evidence of relict or resorption textures. All three porphyroblast minerals overgrow and are included in each other, and boundaries between the three minerals are smooth and curvilinear, indicating their equilibrium co-stability

Table 1. Summary of THERMOCALC Data[a]

Sample	GPS Location[b]	Phases Included in Calculation[c]	Phases Excluded[d]	Activities Excluded[e]	# of Independent Reactions	Minimum σ_{fit} for 95% Confidence	Calculated σ_{fit}	*P* (kbar)	*T* (°C)
10JG181	590009, 6523091	Bt+Ms+Pl+St+Grt+Ky	--	Pg	8	1.45	1.19	10.8±0.9	613±25
10JG182	590031, 6523126	Ms+Pg+Pl+Grt+Amph+Ep	--	Pg, Ms, Parg, Gl	7	1.49	0.94	11.6±1.0	626±25
10JG184	590096, 6523126	Bt+Ms+Pl+Ep+Grt	Kfs, Ttn	Pg	6	1.54	1.22	11.9±1.3	624±45
10JG191-1	590288, 6523163	Bt+Pl+Kfs+Grt+Ep	Ms, Ttn, Ap	--	4	1.73	0.29	12.3±1.0	682±34
10JG191-2	590288, 6523163	Bt+Pl+Kfs+Grt+Ep	Amph	--	4	1.54	0.12	11.4±0.9	664±35

[a]Note: All mineral compositions for thermobarometry were measured on a Cameca SX-100 microprobe at UC-Davis, and all THERMOCALC analyses were completed in THERMOCALC version 3.33 with the thermodynamic data set of *Holland and Powell* [1998].
[b]UTM Zone 19S.
[c]All calculations also included pure quartz and water.
[d]Phases were excluded from the calculation if they showed evidence of textural disequilibrium with the metamorphic assemblage.
[e]Activities were excluded from the calculation if they resulted in consistently high *e** values [*Powell and Holland*, 1994] and if their exclusion did not significantly change the calculated *P-T* result.

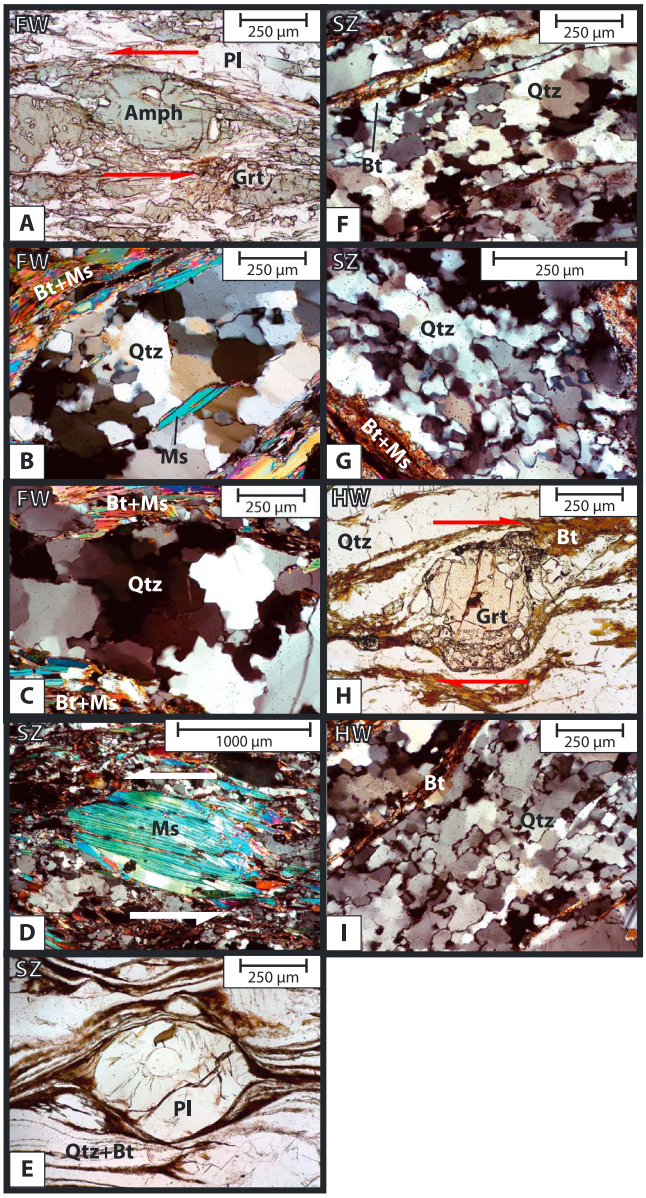

Figure 7. Deformation textures in the BPSZ. Photomicrographs are labeled as footwall (FW), hanging wall (HW), or shear zone (SZ). (a) Kinked, sigmoidal amphibole grains in the footwall indicate a top-to-the-west shear sense (*10JG182*, PPL). (b) Static annealing and GBAR are the dominant quartz textures in the footwall (*10JG181*, XPL). (c) Lobate grain boundaries and strain-free subgrains provide limited evidence of an earlier phase of mixed subgrain-rotation (SGR) and grain-boundary migration (GBM) recrystallization in the footwall (*10JG184*, XPL). (d) Top-to-the-west muscovite mica fish from the base of the shear zone (*10JG185*, XPL). (e) Symmetric, phi-type feldspar porphyroclast from a sample of hanging-wall protolith within the shear zone (*10JG193*, PPL). (f) Grain-boundary migration (GBM) dominated quartz fabrics from the base of the shear zone; subgrain rotation (SGR) shows limited activity (*10JG185*, XPL). (g) Quartz fabrics from the sample closest to the center of the shear zone show mixed GBM/SGR activity (*10JG193*, XPL). (h) Top-to-the-west, stair-stepping biotite pressure shadows around hanging wall garnet (*10JG191-1*, PPL). (i) Quartz deformation was accommodated by grain-boundary migration (GBM) recrystallization in the hanging wall; evidence for SGR is rare (*10JG191-1*, XPL).

[cf. *Vernon et al.*, 2008]. Abundant mica growth across the foliation and annealed quartz fabrics indicate that heating and metamorphism outlasted the latest phase of deformation. Using an average of coarse garnet rim and matrix mineral compositions from pressure shadows, the intersection of eight independent reactions in THERMOCALC records *P-T* conditions of 10.8 ± 0.9 kbar and 613 ± 25°C.

Structurally higher but still ~100 meters below the shear zone in the footwall, a Grt-Czo-Ms-Pg-Amph-Pl-Qtz banded gneiss (sample 10JG182) also records two stages of garnet growth. Garnet cores show sector or concentric zoning, and a sharp resorption surface separates the cores from prograde, concentrically-zoned rims with decreasing Sps and Alm and increasing Prp and Grs. These rims locally overprint the foliation and suggest a late, postkinematic metamorphic episode, which is also implied by overprinting clinozoisite and paragonite grains. The green bands of the gneiss are dominantly composed of amphibole, which shows a pronounced S-C fabric (Figure 7a); garnet, plagioclase, and muscovite are restricted to this layer. Clinozoisite, paragonite, amphibole, and quartz are found in both white and green domains. Though minerals from both gneissic bands were found to be chemically indistinguishable, mineral compositions for thermobarometry were selected exclusively from the green domain to ensure equilibrium with garnet, plagioclase, and muscovite. Combining garnet and amphibole rim averages and matrix mineral compositions, the intersection of seven independent reactions in THERMOCALC resulted in *P-T* conditions of 11.6 ± 1.0 kbar and 626 ± 25°C.

A Grt-Ep-Bt-Ms-Qtz-Pl-Kfs-Ttn calc-pelite schist (sample 10JG184) from ~50 m structurally below the edge of the high-strain zone exhibits a finer grain size and a weak S-C fabric that did not achieve mylonitic conditions. Two stages of prograde garnet growth are

recorded, as in 10JG181 and 10JG182, though X-ray chemical zoning patterns show that prekinematic cores are significantly rarer, perhaps related to increasing grain size reduction and recrystallization with proximity to the shear zone. Epidote porphyroblasts are deformed, but rims overprint the foliation, and inclusions of epidote in garnet rims (and vice versa) show smooth equilibrium boundaries indicative of coexisting phases. Most other matrix minerals show equilibrium relationships with garnet and epidote, but titanite and K-feldspar both show evidence of resorption and are excluded from the thermodynamic calculation. Using an average of garnet rim points and matrix mineral compositions, the intersection of six independent reactions in THERMOCALC gives *P-T* conditions of 11.9 ± 1.3 kbar and 624 ± 45°C.

4.2.2. Shear Zone

An attempt was made to constrain *P-T* conditions within the shear zone from pelitic mylonite samples 10JG188-1-B and 10JG188-2 (Grt-Ep-Bt-Ms-Pl-Kfs-Qtz ± Ttn ± St). However, mineral textures were not indicative of metamorphic equilibrium; as such, THERMOCALC results were consistently above the maximum σ_{fit} predicted by the assemblage, and the calculated *P-T* conditions varied significantly with the inclusion or exclusion of various components. The poor THERMOCALC fit to the chemical data suggests that metamorphic minerals within the shear zone did not achieve thermodynamic equilibrium during or subsequent to deformation.

4.2.3. Hanging Wall

A Grt-Ep-Bt-Ms-Pl-Qtz-Kfs-Ttn-Ap orthogneiss (sample 10JG191-1) from the hanging wall Bajo Pequeño Gneiss (~45 m above the top of the BPSZ) suggests a transition to a simpler metamorphic history in the hanging wall. Garnet porphyroblasts lack internal inclusion fabrics, are wrapped by the foliation (Figure 6c), and show only a single, prograde, synkinematic growth episode (Figure 6d) coincident with pressure shadow development. All other matrix minerals either define or are wrapped by the foliation, with no postkinematic growth. Mineral compositions for thermobarometry were selected from garnet rims, associated pressure shadows (Bt-Pl-Kfs-Qtz), and local foliation-forming mica. Muscovite, titanite, and apatite were excluded due to textural evidence suggesting disequilibrium with respect to the latest episode of garnet growth. The intersection of four independent reactions in THERMOCALC between the remaining components resulted in *P-T* conditions of 12.3 ± 1.0 kbar and 682 ± 34°C.

Sample 10JG191-2 (Grt-Ep-Amph-Bt-Qtz-Pl-Kfs) also records a one-stage metamorphic history. Only two anhedral, millimeter-sized garnet grains were noted in thin section, and both are strongly deformed and wrapped by the foliation with biotite pressure shadows. These garnets show only a single phase of prograde growth. Textural relationships between other minerals in the sample are similar to those in 10JG191-1, with most porphyroblasts wrapped by the foliation. Amphibole, not present in 10JG191-1, is highly deformed into mineral fish. Using chemical data from all phases except amphibole (due to textural disequilibrium) and adding H_2O, four independent reactions intersected in THERMOCALC resulting in *P-T* conditions of 11.4 ± 0.9 kbar and 664 ± 35°C.

4.3. Summary

Metamorphic and thermobarometric data from the Bajo Pequeño Shear Zone indicate a slight, inverted thermal gradient from footwall to hanging wall during the latest stages of metamorphism, with footwall temperatures averaging 620 ± 16°C (MSWD = 0.29) and hanging wall temperatures averaging 673 ± 24°C (MSWD = 0.59). Calculated pressures are within error across both units (11–12 kbar). The footwall preserves two distinct stages of garnet growth, but the hanging wall only preserves a single phase of metamorphism, as observed in garnet chemical zoning patterns. However, though both footwall and hanging wall record equilibrium mineral growth during metamorphism, the shear zone itself did not equilibrate due to continued deformation. These data indicate that (1) units demarcated by the BPSZ experienced different metamorphic and thermal histories prior to their juxtaposition by the shear zone, and (2) the earliest stages of shear zone development were characterized by a thermal gradient from footwall to hanging wall.

5. Deformation Textures and Quartz Fabrics

In order to clarify the relationship of deformation to metamorphism, samples from below, within, and above the shear zone were analyzed for characteristic deformation fabrics in thin section. In addition, quartz *c*-axis fabrics were measured using electron backscatter diffraction (EBSD) analysis [e.g., *Prior et al.*, 1999; *Maitland and Sitzman*, 2007].

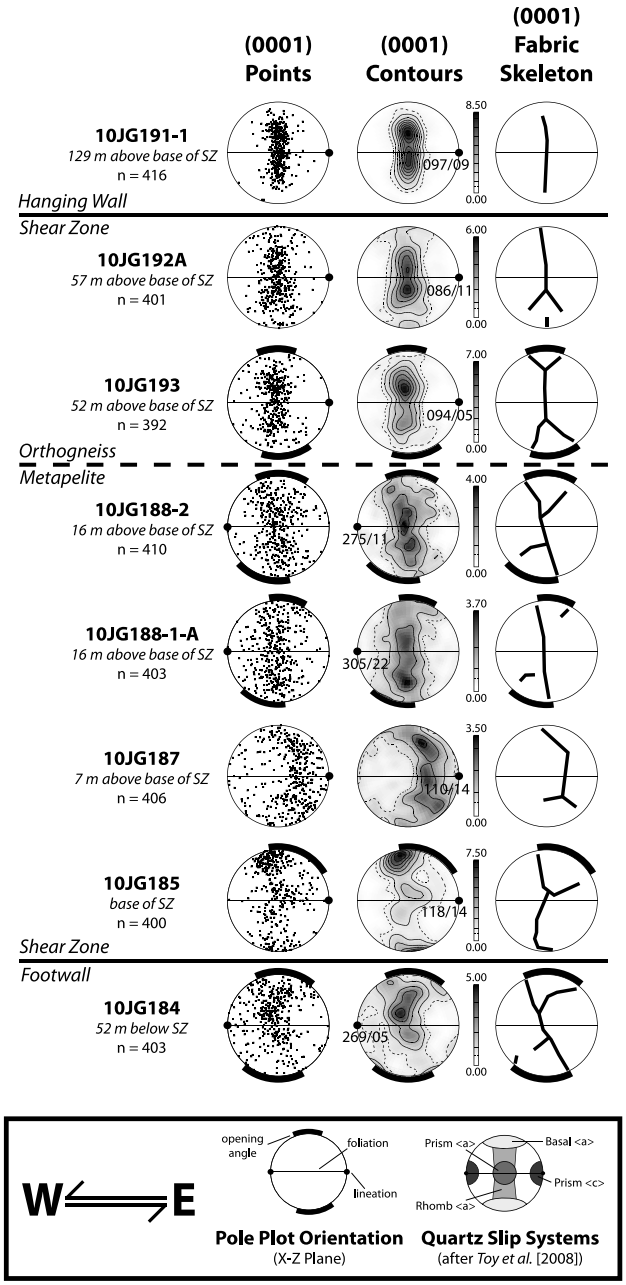

Figure 8. Summary of quartz *c*-axis data. Lower hemisphere, equal area pole figures were produced in PFChannel5 software provided by D. Mainprice. For each contour plot, a dashed contour marks 0.5 times a uniform distribution and solid contours mark integer units relative to multiples of a uniform distribution of the maximum concentration (shown with each plot). Plots are oriented perpendicular to the foliation (shown as an E-W line) and parallel to lineation (shown as a dot in the downdip direction of the foliation plane); all samples have a mylonitic foliation except for 10JG184, and sample 10JG191-1 also exhibits gneissic banding at outcrop. All samples have been rotated so that the sinistral shear direction is top-to-the-west. Opening angles are shown as a black bar on the edge of the pole plot; the correlation between *c*-axis orientations and quartz slip systems (modified after *Toy et al.* [2008]) is shown for reference. The plots show a transition from crossed girdles affected by simple shear in the metapelite to single, symmetric girdles indicative of higher-temperature slip systems and more coaxial shear in the orthogneiss, above the compositional boundary.

5.1. Methods

Deformation textures were analyzed using a petrographic microscope at UC-Davis. An FEI Quanta 200 W scanning electron microscope (SEM) with an HKL Technologies EBSD detector, affiliated with the Warren lab at Stanford University, was used for all quartz *c*-axis work. Samples were analyzed with a 20 kV accelerating voltage and a current set to 7 under low-vacuum conditions (30 Pa H_2O). Data were collected and processed using the HKL Channel5 software package. Approximately 400 quartz *c*-axis orientations were collected from each thin section by completing manual traverses along quartz-rich bands and stringers. Points with a mean angular deviation (MAD) of >1° from the simulated fit were discarded from the data set.

Pole figures of *c*-axis data were plotted using the PFChannel5 software of D. Mainprice. All pole figures are lower hemisphere, equal area projections. *C*-axis opening angles were estimated by determining the arc between the center points of each girdle arm, and angles were measured around the *X* axes of the pole plot and averaged (Figure 8). Opening angles were matched to deformation temperatures using the empirical *Kruhl* [1998] thermometer, as modified by *Law et al.* [2004] and *Morgan and Law* [2004] (see Figure 9). An error of ±50°C is attached to each measurement to encompass variability in strain rates and hydrolytic weakening under natural deformation conditions [*Kruhl*, 1998; *Law et al.*, 2004], and uncertainty in opening angle estimation.

5.2. Results: Deformation Textures

5.2.1. Footwall

Samples from the Duraznos Complex are primarily characterized by static recrystallization textures. However, deformation textures become apparent with proximity to the shear zone, e.g., a penetrative top-to-the-west S-C fabric in 10JG182 and 10JG184. Other kinematic indicators also record top-to-the-west shear and include stair-stepping pressure shadows, sigmoid amphibole clasts

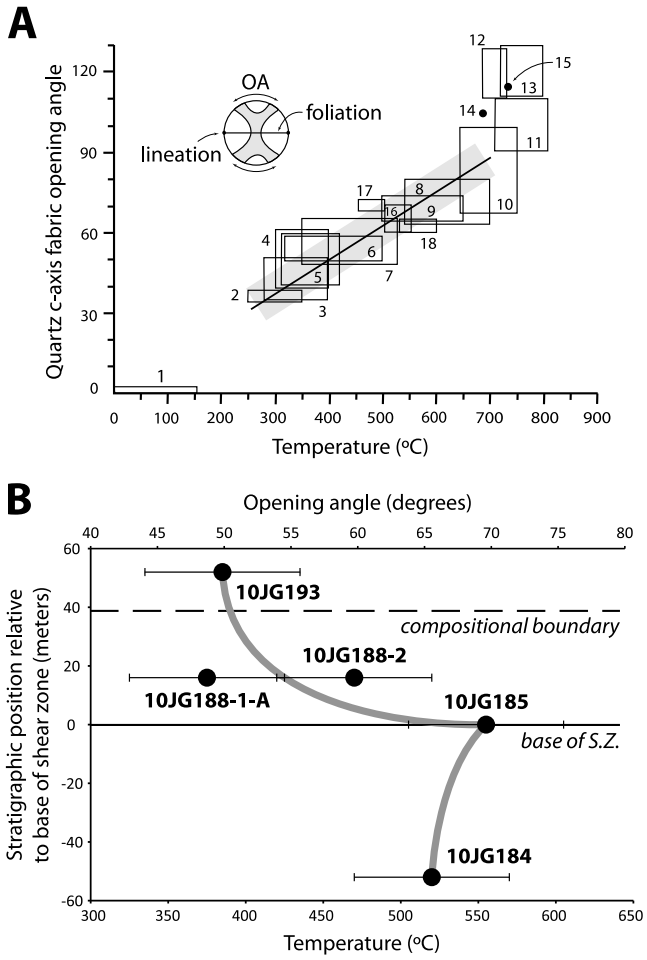

Figure 9. Quartz *c*-axis opening angles and deformation temperature. (a) The *Kruhl* [1998] thermometer, modified by *Law et al.* [2004], that is used to correlate the pole plot opening angle for quartz *c* axes to the temperature of deformation. The thermometer is based on empirical data, assumes plane strain deformation, and has an error of ± 50°C. Figure modified from *Law et al.* [2004]. (b) Opening angles (bottom scale) and deformation temperatures (top scale) for BPSZ samples plotted with their stratigraphic level relative to the base of the shear zone (identified as "zero elevation" and marked with a solid black line). Only samples with crossed girdles are shown, so the plot does not include the upper part of the shear zone or the hanging wall. The compositional boundary in the center of the shear zone is identified by a dashed black line. The opening angles record higher temperatures in the footwall and the lowest temperatures in the core of the shear zone; the solid gray line marks a rough fit to the available data.

(Figure 7a), and micaceous (Bt + Ms ± Pg) shear bands and mineral fish. Plagioclase (±Kfs) is common in all footwall samples; dynamic recrystallization in the grain-boundary bulging (BLG) regime is observed in larger grains, though well-developed core-and-mantle structures are rare. Contacts between plagioclase subgrains contain fine-scale mica splays, suggesting fluid activity during retrogression.

Quartz is present as stringers, bands, and deformed aggregates. Static recrystallization is dominant, particularly grain boundary area reduction (GBAR), as evidenced by ubiquitous 120° grain junctions (Figure 7b). This annealing overprints an earlier phase of mixed subgrain rotation (SGR) and grain boundary migration (GBM) recrystallization (Regime III of *Hirth and Tullis* [1992]), seen in limited domains with highly lobate grains and strain-free, misaligned subgrains with straight boundaries (Figure 7c). Quartz lacks a shape-preferred orientation (SPO) in all footwall samples, but the addition of a gypsum plate reveals a weak lattice-preferred orientation (LPO) that increases in intensity with proximity to the shear zone (Figure 8).

5.2.2. Shear Zone

Samples 10JG185, 10JG187, 10JG188-1-A, and 10JG188-2 are located below the compositional boundary (Figure 4) and are dominantly metapelitic; samples 10JG193 and 10JG192A are metaigneous with different modal fractions of mica.

A top-to-the-west shear sense is unambiguous at the base of the shear zone, defined by mineral porphyroclasts and fish (Figure 7d), stair-stepping pressure shadows, and shear bands. However, with increasing distance upsection, porphyroclasts transition from σ-type (asymmetric) to φ- and θ- type (symmetric), pressure shadows and porphyroclast tails cease to show any stair stepping (Figure 7e), and a set of conjugate shear bands are developed that intersect each other. The samples at the top of the shear zone show no clear shear sense for the above kinematic indicators.

Though brittly-deformed garnet and amphibole are common, plastically-deformed feldspar (Pl + Kfs) porphyroclasts are most indicative of the change from σ-type to φ- and θ-type with increasing distance upsection. Core-and-mantle structures are abundant and indicative of grain-boundary bulging recrystallization (BLG). Numerous subgrain boundaries and "leftover" spots within feldspar [e.g., *Passchier and Trouw*, 2005] suggest the possible influence of SGR recrystallization.

Quartz is present as 100% recrystallized bands and ribbons parallel to the foliation, and in some samples as a fine-grained disseminated phase mixed with feldspar and mica. Recrystallization textures are complex but dominated by mixed SGR and GBM (Regime III of *Hirth and Tullis* [1992]). The sample at the base of the shear zone (10JG185) shows an oblique top-to-the-west quartz inclination deformed dominantly by GBM with only minor SGR (Figure 7f). In contrast, the sample closest to the center of the shear zone (10JG193) indicates an earlier phase of GBM overprinted by SGR, as the outlines of larger, more lobate grains are broken down into misaligned subgrains (Figure 7g). Sample 10JG193 also shows strained ribbons with an SPO that is parallel to the foliation or inclined in a top-to-the-west direction. Most grains within these stringers show high strain with no evidence of recovery. However, there is appreciable GBAR and recovery at the edges of the shear zone (10JG185 and 10JG192A). This annealing is localized even on a millimeter scale: many stringers and ribbons show no evidence for it though some show a characteristic foam texture. All samples from the shear zone have a quartz LPO (Figure 8).

5.2.3. Hanging Wall (10JG191-1)

The metaigneous hanging wall records gneissic banding with S-C fabric present in more micaceous layers. Shear sense is unambiguously top-to-the-west, as indicated by sigmoid mineral porphyroclasts and fish, stair-stepping pressure shadows, and micaceous shear bands (e.g., Figure 7h). Feldspar (Pl + Kfs) is present as deformed, sigmoid porphyroclasts with undulose extinction, and larger grains show core-and-mantle structures indicative of bulging recrystallization (BLG). Quartz is restricted to 2–3 mm bands with a minor, foliation-parallel, or slightly oblique SPO; a clear LPO is developed within these layers (Figure 8). Lobate and sutured grain boundaries indicative of GBM-only recrystallization are most abundant (Figure 7i). SGR microstructures are subsidiary and are nonexistent across much of the sample. Annealing and GBAR are uncommon and generally restricted to specific areas of the thin section.

5.2.4. Summary of Deformation Textures and Kinematic Indicators

The footwall Duraznos Complex samples record a period of high-*T*, top-to-the-west, asymmetric shear that was overprinted by metamorphic and static annealing, indicating that footwall deformation ceased relatively early in the history of the shear zone. The mylonitic shear zone samples, in contrast, record mineral textures that indicate intense deformation to lower temperatures or higher strain rates, a transition from asymmetric to symmetric shear from the base to the top of the shear zone, and minor annealing at the edges of the shear zone, all of which suggest localization of strain with time. The sample from the hanging wall Bajo Pequeño Gneiss shows deformation textures that were attained at high temperatures and then subject to limited static recrystallization.

5.3. Results: Quartz Pole Plots and *C*-Axis Opening Angles

Quartz *c*-axis patterns determined by EBSD provide more quantitative constraints on deformation temperatures and the thermal evolution of the shear zone. In particular, the active slip systems in quartz vary with temperature, among other factors [*Toy et al.*, 2008] (Figure 8). Likewise, quartz *c*-axis opening angles have been empirically correlated with deformation temperature [*Kruhl,* 1998*; Law et al.,* 2004] (Figure 9) as well as strain rate [e.g.*, Tullis et al.*, 1973; *Hirth and Tullis*, 1992]. Quartz *c*-axis distributions can also qualitatively support textural interpretations of shear sense and structural style of deformation [e.g., *Passchier and Trouw*, 2005]. Note that the opening angle thermometer requires plane strain deformation [*Kruhl*, 1998; *Law et al.*, 2004], but the Type I crossed girdles in our samples (below) suggest that this assumption is justified here [*Passchier and Trouw*, 2005].

The footwall (10JG184) records an asymmetric, Type I crossed girdle [e.g., *Lister*, 1977] with mixed basal, rhomb, and prism $<$ a $>$ slip, consistent with top-to-the-west deformation under plane strain simple shear conditions [e.g., *Schmid and Casey*, 1986]. The opening angle recorded by this sample (66°) corresponds to a deformation temperature of 520 ± 50°C.

The lower part of the shear zone (10JG185, 10JG187, 10JG188-1-A, and 10JG188-2) records a transition from Z-maxima (dominated by basal $<$ a $>$ slip) at the edge of the shear zone to Type I crossed girdles upsection (mixed $<$ a $>$ slip). Girdle opening angles correspondingly decrease from the edge of the shear zone (70°) to the center (47–59°). These fabrics all show top-to-the-west asymmetry and are inclined in the shear direction toward the foliation plane. Using those samples that display viable opening angles, the progressive decrease in opening angle magnitude from the base to the core of the shear zone corresponds to decreasing deformation temperatures, from 555 ± 50°C to 375–470 ± 50°C.

The upper part of the shear zone (10JG193 and 10JG192-A) records single girdles with mixed prism and rhomb < a > slip, but lacking a basal < a > component. A weak crossed-girdle fabric in sample 10JG193 records an opening angle (49°) corresponding to a deformation temperature of 385 ± 50°C. Both *c*-axis patterns are nearly symmetric about the *X-Y* plane.

The hanging wall (10JG191-1) records a well-defined single girdle entirely lacking a basal < a > component of slip, with no sense of shear asymmetry. No opening angle can be measured from this sample.

In summary, quartz *c*-axis patterns from the BPSZ indicate (1) a transition from mixed basal, rhomb, and prism < a > slip in the footwall and base of the shear zone to solely rhomb and prism < a > slip in the upper part of the shear zone and hanging wall; (2) a transition from asymmetric Type I crossed girdles in the footwall and base of the shear zone to symmetric single girdles in the upper part of the shear zone and hanging wall; and (3) opening angles in those samples with Type I crossed girdles that show falling deformation temperatures or increasing strain rates from the edge of the shear zone to its core.

6. $^{40}Ar/^{39}Ar$ Thermochronology

Two hornblende and two white mica separates were dated by the $^{40}Ar/^{39}Ar$ method in order to assess the timing of activity along the BPSZ. Amphibole and muscovite were selected because their closure temperatures (~550–500°C and ~425–350°C, respectively, depending on cooling rate and composition) [e.g., *Dahl*, 1996; *Harrison et al.*, 2009] span the range of temperatures over which the BPSZ was active, from the lower bound of metamorphism to the coolest deformation temperatures.

6.1. Methods

Samples were hand crushed, sieved, run through a Frantz magnetic separator, and picked at UC-Davis. The samples were irradiated for 50 h in the Cadmium-Lined in-Core Irradiation Tube (CLICIT) facility of the Oregon State University Triga Reactor, along with the Fish Canyon sanidine standard in an Al disk as described by *Renne et al.* [1998]. Standards from four positions spanning the disk yielded an average *J*-value (a measure of the fast neutron fluence) of $(1.3047 \pm 0.0002) \times 10^{-2}$. Samples comprising ~20 grains of hornblende (100–250 μm diameter for 10JG191-2 and 300-600 μm for 10JG182) and ~5 grains of muscovite (300–600 μm for both samples) were analyzed by incremental heating in 9–15 steps with the defocused beam from a CO_2 laser following methods described by *Mulcahy et al.* [2011]. All sample analyses were completed at the Berkeley Geochronology Center and ages are based on the calibration of *Renne et al.* [2011]. Full analysis tables for all $^{40}Ar/^{39}Ar$ samples are contained in the supporting information. All reported errors for this method are ±2σ.

6.2. Results

6.2.1. Footwall Hornblende and White Mica

Both hornblende and white mica were analyzed from the footwall Grt-Czo-Ms-Pg-Amph-Pl-Qtz banded gneiss (cf. section 4.2.2). Na- and Fe-rich hornblende occurs as coarse sigmoid clasts and preserves a top-to-the-west S-C fabric (Figure 7a). The hornblende ^{39}Ar-release spectrum (Figure 10a) does not define a single plateau age, and steps fluctuate with increasing power. The low-*T* end of the spectrum shows evidence for excess ^{40}Ar (resulting in an older apparent age) accompanied by depressed Ca/K ratios, the effect of which decreases progressively with the first five steps. These first five steps likely indicate contamination by another phase, which is also suggested by X-ray maps showing K-rich phases along cracks in hornblende grains. An inverse isochron plot does not yield a statistically significant age or well-defined excess Ar composition, as the spread in $^{39}Ar/^{40}Ar$ among heating steps is minimal. Therefore, we do not report an age for this sample.

Muscovite and paragonite occur throughout the sample as needles and mineral fish; in the green domain they appear concordant with the foliation (synkinematic) but in the white domain, numerous splays of paragonite clearly overprint the foliation (postkinematic). The two phases could not be distinguished during the mineral separation process, and therefore, the analyzed grains include both mica types. The Ar step-heating spectrum (Figure 10c) results in a single-plateau age over 100% of the ^{39}Ar gas released, with a $^{40}Ar/^{39}Ar$ age of 404 ± 3 Ma (MSWD = 0.51). Given that metamorphic temperatures for this sample (~625°C) exceed expected white mica closure temperatures, this age is interpreted to record cooling after white mica neocrystallization and recrystallization during shear zone activity and footwall metamorphism.

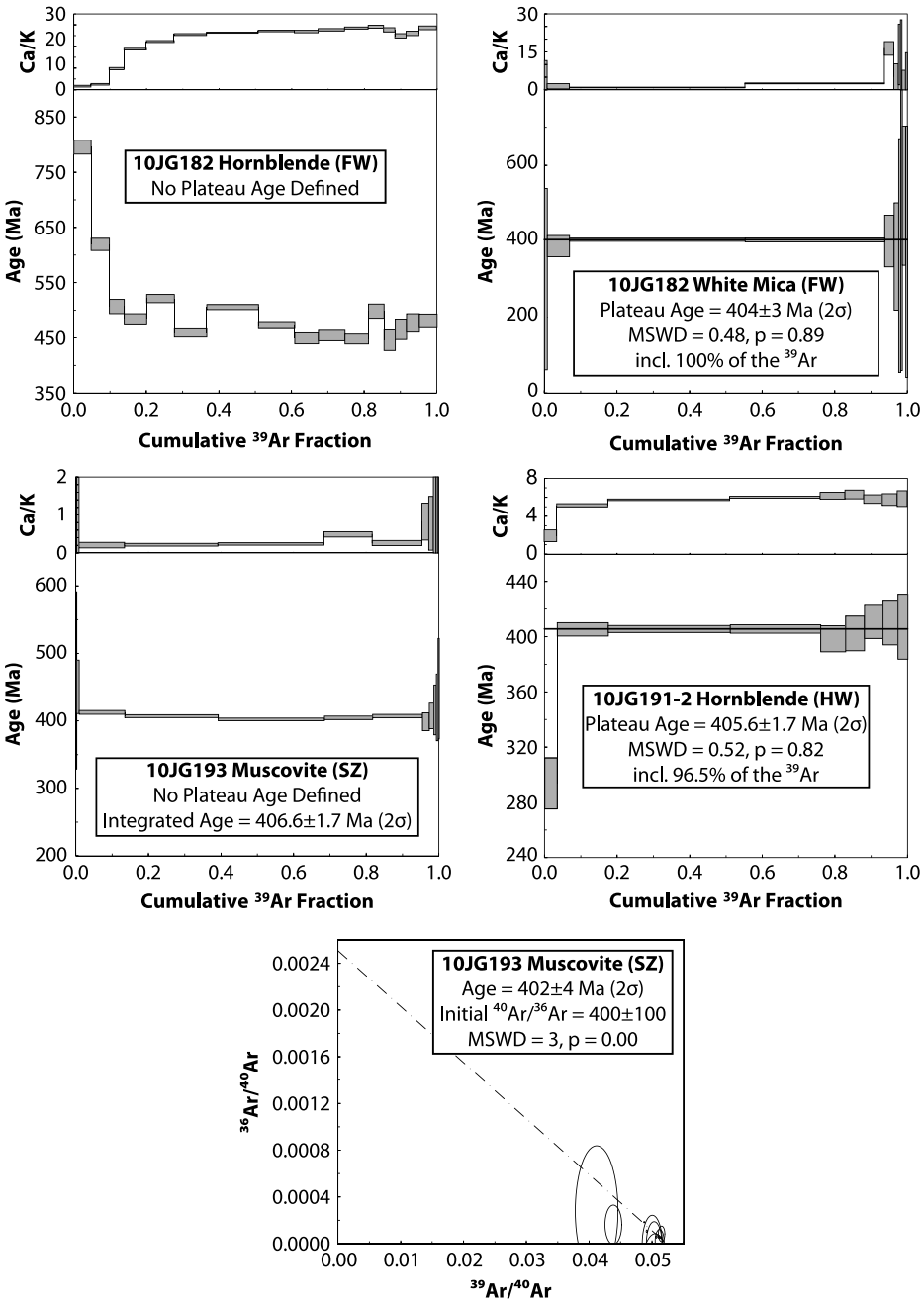

Figure 10. ^{40}Ar/^{39}Ar ages, labeled as footwall (FW), hanging wall (HW), or shear zone (SZ). Age spectra and inverse isochron plots for footwall hornblende and white mica (10JG182), shear zone muscovite (10JG193), and hanging wall hornblende (10JG191-2). Analysis tables used to produce these plots can be found in the supporting information.

6.2.2. Shear Zone Muscovite

This Ep-Ms-Bt-Pl-Qtz mylonite preserves coarse muscovite (>200 μm) as deformed mineral fish. The Ar step-heating spectrum does not define a single plateau age over the majority of the released ^{39}Ar; steps cluster between 400 and 410 Ma with an integrated age of 406.6 ± 1.7 Ma (Figure 10d). However, an inverse isochron plot (Figure 10e) reveals a ^{40}Ar/^{39}Ar "errorchron" age of 402 ± 4 Ma (MSWD = 3) with a ^{40}Ar/^{36}Ar intercept of 400 ± 100, close to the atmospheric value of 296. Considering our temperature constraints on metamorphism and deformation, we interpret this age as recording the cooling of neocrystallized muscovite during shear zone activity.

6.2.3. Hanging Wall Hornblende

This Grt-Ep-Amph-Bt-Qtz-Pl-Kfs felsic orthogneiss (cf. section 4.2.3) contains strongly deformed, fractured ferroan hornblende that is interstitial to feldspar porphyroclasts. Mineral separates for this sample were taken from an earlier separate produced for zircon dating by *Austin et al.* [2011], and therefore were chosen from a smaller size fraction (45–250 μm) than for 10JG182 (300–600 μm); however, all analyzed grains were >100 μm. The Ar step-heating spectrum (Figure 10f) defines a plateau age over 96.5% of the released ^{39}Ar, resulting in a ^{40}Ar/^{39}Ar age of 405.6 ± 1.7 Ma (MSWD = 0.52). Because the metamorphic *P-T* conditions calculated for this sample exceed hornblende closure temperatures by 100–125°C, we interpret this age as recording cooling of the orthogneiss below hornblende closure.

6.3. Summary

^{40}Ar/^{39}Ar cooling ages from the BPSZ indicate that (1) white mica from the footwall Duraznos Complex records a phase of growth, recrystallization, and subsequent cooling at 404 ± 3 Ma; (2) the hanging wall Bajo Pequeño Gneiss cooled below the hornblende closure temperature at 405.6 ± 1.7 Ma; and (3) mylonites from the shear zone cooled below the muscovite closure temperature by 402 ± 4 Ma. Because the muscovite and hornblende cooling ages overlap within analytical uncertainty, despite having a closure temperature difference of 100–150°C, we interpret these ages as recording relatively rapid cooling during exhumation.

7. U-Pb SHRIMP Zircon Geochronology

Zircons from the hanging wall Bajo Pequeño Gneiss were dated by U-Pb sensitive high-resolution ion microprobe (SHRIMP) geochronology to constrain the timing of igneous (protolith) crystallization and subsequent metamorphism of the orthogneiss, particularly to compare its polyphase metamorphic and structural history with that of the footwall Duraznos Complex (as determined by *Mulcahy et al.* [2011] and this work). This unit had been previously investigated using LA-ICP-MS U-Pb zircon dating by *Austin et al.* [2011], who determined a crystallization age of ~1245 Ma. However, though metamorphic overgrowths on zircon were noted, they were not dated. We therefore present an updated crystallization age and a first report of two distinct metamorphic ages for the Bajo Pequeño Gneiss.

7.1. Methods

Zircons for U-Pb SHRIMP analysis were selected from the 45 to 250 μm size fraction of sample 10LA98 which was previously analyzed by LA-ICPMS [*Austin et al.,* 2011] and from the same location as sample 10JG191-2 used in this study. The sample was hand crushed, sieved, run through a Frantz magnetic separator, and handpicked at UC-Davis. Grains were mounted in a 2.54 cm epoxy round, polished to expose the grain interiors, and imaged with transmitted light, reflected light, and cathodoluminescence (CL) (Figure 11a) prior to analysis. U-Pb isotope and trace element compositions were collected simultaneously on the SHRIMP-RG (sensitive high-resolution ion microprobe-reverse geometry) instrument at the U.S. Geological Survey-Stanford University Ion Probe Laboratory using a 25 μm diameter spot size. The U-Pb analytical routine followed *Williams* [1998] and data reduction utilized the SQUID program of *Ludwig* [2001]. U-Pb isotopic composition was calibrated by replicate analyses of zircon standard R33 (419 Ma) [*Black et al.*, 2004], and U concentration was calibrated using zircon standard CZ3 (U = 550 ppm) [*Pidgeon et al.*, 1994]. Calibration errors for ^{206}Pb/^{238}U ratios of R33 for the two analytical sessions were 0.55% and 0.77% (2σ). Ages are calculated as weighted mean ^{207}Pb-corrected ^{206}Pb/^{238}U ages and upper intercept ages based on ^{204}Pb-corrected ratios using the Isoplot/Ex program of *Ludwig* [2003] (Figure 11c). Common Pb compositions were estimated from *Stacey and Kramers* [1975]. Full analysis tables for U-Pb zircon dating are contained in the supporting information.

Trace element data collection was simultaneous with U-Pb analysis following *Mazdab and Wooden* [2006] and *Mattinson et al.* [2009]. The rare-earth element (REE) routine measured ^{139}La, ^{140}Ce, ^{146}Nd, ^{147}Sm, ^{153}Eu, ^{157}Gd^{16}O, ^{163}Dy^{16}O, ^{166}Er^{16}O, ^{172}Yb^{16}O, and ^{180}Hf^{16}O (raw data contained in the supporting information). Concentration calibrations used trace element values of zircon standards CZ3 and MAD [*Mazdab and Wooden,* 2006]. Estimated errors based on repeated analysis of CZ3 are 5–10% for Y, Hf, Th, and U and the REE except for La (30%) and include both analytical reproducibility and real abundance variation in the gem quality zircon [cf. *Mattinson et al.,* 2009]. Chondrite-normalized REE plots (Figure 11b) use the chondrite REE abundances of *Anders and Grevesse* [1989] multiplied by a factor of 1.36 [*Korotev*, 1996]. Chondrite-normalized values for Pr were calculated by interpolation ($Pr_{(N)} = La_{(N)}^{0.33} \times Nd_{(N)}^{0.67}$).

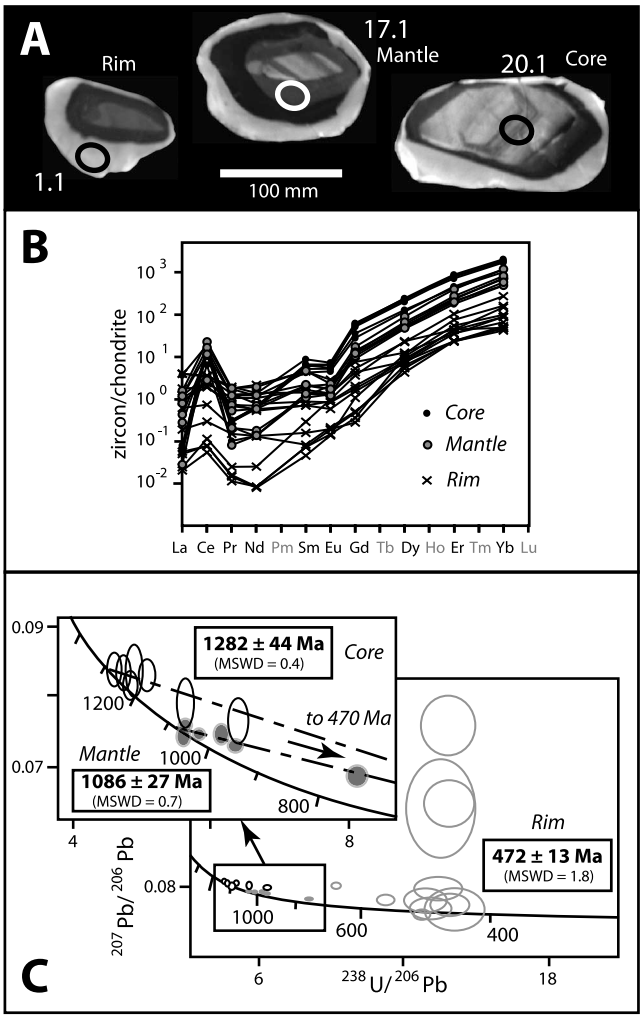

Figure 11. U-Pb SHRIMP ages. (a) Examples of zircons from 10LA98/10JG191-2, with oscillatory zoned cores, CL-dark mantles, and CL-bright rims. The analysis numbers correlate to data contained in the data repository. (b) Distinct REE patterns for each CL domain in zircons from 10LA98/10JG191-2. (c) Tera-Wasserburg U-Pb concordia plot showing that each CL domain also preserves a unique age signature associated with major thermal events.

7.2. Results

The single sample analyzed by this method (10LA98/10JG191-2) is a Grt-Ep-Amph-Bt-Qtz-Pl-Kfs orthogneiss taken from the hanging wall of the BPSZ, above the upper boundary of the shear zone (cf. sections 4.2.6 and 6.2.3). The zircons are subhedral with distinct euhedral oscillatory zoned cores overgrown by CL-dark mantles and outer CL-bright rims (Figure 11a). The cores have REE patterns typical of igneous zircon, whereas both mantles and rims show middle- and heavy-REE depletion; this depletion is more extreme in the rims (Figure 11b). The variation in CL and chemical signatures clearly define multiple domains within the zircon population. The age data from the domains are distinct as well (Figure 11c). Concordant to nearly concordant analyses from the low U rims give a weighted mean $^{206}Pb/^{238}U$ age of 472 ± 13 Ma (MSWD = 1.8), which overlaps with previously reported ages of peak temperature metamorphism in the range [cf. *Casquet et al.*, 2001; *Mulcahy et al.*, 2011]. Assuming a lower intercept of 470 Ma, linear regression of the ^{204}Pb-corrected core analyses gives an upper intercept of 1282 ± 44 Ma (MSWD = 0.4), which is interpreted as the protolith crystallization age and consistent with the age obtained by LA-ICPMS [*Austin et al.,* 2011]. Similar regression of analyses from the mantles gives an upper intercept of 1086 ± 27 Ma (MSWD = 0.7), which is inferred to record the timing of a Mesoproterozoic metamorphic event.

8. Discussion

8.1. *P-T-t* Histories of the Footwall (Duraznos Complex), Hanging Wall (Bajo Pequeño Gneiss), and the BPSZ

The distinct geologic histories of the footwall and hanging wall establish the BPSZ as a significant lower-crustal structure that likely accommodated tens of kilometers of displacement. Footwall Duraznos Complex metasediments were deposited at or after 966 ± 36 Ma [*Austin et al.*, 2011] and exhibit two stages of metamorphic mineral growth, with the most recent postkinematic assemblage recording ~11 kbar and ~620°C conditions. Previous geochronology and thermochronology from a structurally deeper footwall sample by *Mulcahy et al.* [2011] indicate that prekinematic garnet cores grew at 469 ± 21 Ma (Lu-Hf), whereas synkinematic hornblende and muscovite cooled through their argon closure temperatures at 441 ± 16 Ma and 436 ± 4 Ma, respectively. Importantly, the sample dated by *Mulcahy et al.* [2011] is <500 m downsection from the BPSZ (Figure 3) yet preserves no postkinematic garnet rims. Only rocks in the immediate footwall of

the BPSZ recorded this late-stage static metamorphism associated with overthrusting of the hotter orthogneiss, likely assisted by deformation- and fluid-controlled reequilibration [e.g., *Kuhn et al.,* 2000; *Bjørnerud and Austrheim,* 2002] or shear heating [e.g., *Camacho et al.*, 2001; *Camacho*, 2002]. However, we consider the latter process minor because the BPSZ was unlikely to have sustained the high stresses required for significant dissipative heating [cf. *Kidder and Ducea*, 2006]. Furthermore, in contrast to studies in which shear zone fabrics show higher temperatures than their wall rocks [e.g., *Camacho et al.*, 2001; *Camacho,* 2002], the BPSZ shows shear zone fabrics that were deformed at lower temperatures than their wall rocks (section 8.2.3, below), suggesting that the effects of shear heating were limited.

Evidence for localized heating and reequilibration is reinforced by our new footwall Ar/Ar data that show complete recrystallization and resetting of white mica (404 ± 3 Ma, sample 10JG182) in proximity to the shear zone. The spatial correlation in the footwall between postkinematic metamorphic mineral growth and the reset white mica Ar/Ar age near the BPSZ, and their absence in the same package downsection, suggests that the postkinematic *P-T* conditions determined in this study were acquired in a reheating event *after* partial exhumation at 436 ± 4 Ma. Taken together, these data require that the Duraznos Complex was metamorphosed at lower-crustal conditions (9.3 ± 0.8 kbar and 638 ± 15°C) by 469 ± 21 Ma [*Mulcahy et al.*, 2011], exhumed or cooled below muscovite closure by 436 ± 4 Ma [*Mulcahy et al.*, 2011], and reburied and reheated to lower crustal conditions (11.3 ± 0.6 kbar and 620 ± 16°C) between 435 and 405 Ma.

The geologic history of the hanging wall Bajo Pequeño Gneiss suggests that it evolved separately from the Duraznos Complex prior to juxtaposition along the BPSZ. Our new U-Pb data from sample 10JG191-2 support the Mesoproterozoic (~1245 Ma) crystallization age determined by *Austin et al.* [2011] and also indicate a Grenville metamorphic event (1086 ± 27 Ma) that occurred prior to deposition of the Duraznos Complex. This latter metamorphic age is similar to other igneous and metamorphic ages from the Pie de Palo Complex structurally downsection (Figure 3) [*Vujovich et al.*, 2004; *Mulcahy et al.*, 2011], but the crystallization age of the Bajo Pequeño Gneiss is significantly older than crystallization ages for rocks of the Pie de Palo Complex, all of which are younger than ~1200 Ma [*Vujovich et al.*, 2004; *Rapela et al.*, 2010]. Synkinematic mineral assemblages in the Bajo Pequeño Gneiss record only a single metamorphic episode culminating in *P-T* conditions of ~12 kbar and ~675°C; the timing of this metamorphism is indicated by our zircon rim weighted mean age of 472 ± 13 Ma. However, there is no thermochronologic evidence for exhumation or cooling of the hanging wall at 440–435 Ma, in contrast to the footwall rocks that cooled below muscovite closure at that time [*Mulcahy et al.*, 2011]. Additionally, our textural observations suggest that the hanging wall must have remained hot until ~405 Ma to explain the thermal gradient from footwall to hanging wall during the earliest stages of BPSZ activity. As such, we posit that the *P-T* conditions calculated from our hanging wall samples persisted in the orthogneiss from ~470 Ma until exhumation initiated along the BPSZ.

A comparison between metamorphic temperatures and muscovite closure temperatures therefore suggests that the hanging wall Bajo Pequeño Gneiss was at least ~250°C hotter than the partially exhumed Duraznos Complex at 440–435 Ma, ~30 Myr prior to their juxtaposition by the shear zone. Assuming that a "normal" geothermal gradient (e.g., 30°C/km) was reestablished after subduction ceased along the Gondwana margin, these units may still have been at crustal depths that were up to 10 km apart. However, lateral separation and fluctuating geotherms during crustal shortening could also explain the temperature differences, and it is therefore difficult to determine their exact pre-BPSZ crustal levels.

Once movement along the shear zone commenced, the hanging wall cooled below ~550°C at 405.6 ± 1.7 Ma (sample 10JG191-2), corresponding to the high-temperature limit of preserved deformation textures in the BPSZ. Muscovite ages from the shear zone (402 ± 4 Ma, sample 10JG193) and the footwall (404 ± 3 Ma, sample 10JG182) record cooling below ~400°C, and therefore date the latest stages of activity along the shear zone [e.g., *Dunlap*, 1997] and metamorphism and annealing in the footwall. Because these cooling ages are among the youngest in the Pie de Palo, we posit that they represent the cessation of significant lower-crustal deformation and indicate final exhumation of both units to the middle crust. The overlap between the hornblende and muscovite $^{40}Ar/^{39}Ar$ ages indicates fast cooling during exhumation, which is supported by our thermometry and microstructural data from the shear zone, especially the preserved inverted thermal gradient [cf. *England and Molnar*, 1993]. Potential cooling rates range from ~20 to 200°C/Ma, which suggests that Ar-system closure temperatures are on the high end of their possible ranges [e.g., *Dahl*, 1996].

8.2. Characterization of Structural Activity Along the BPSZ

8.2.1. Mineral Fabrics Provide General Estimates of Deformation Temperature

Petrographic observations from the units along the BPSZ provide broad constraints on the range of deformation temperatures recorded by the shear zone. Quartz textures in the SGR and GBM field for all samples (Figure 7) indicate temperatures >400°C [e.g., *Stipp et al.*, 2002; *Faleiros et al.*, 2010], but the lack of prism [c] slip in the section (Figure 8) constrains deformation to a temperature maximum of 550–600°C [*Okudaira et al.*, 1995; *Takeshita*, 1996; *Stipp et al.*, 2002]. Brittle garnet and amphibole deformation support 600°C as the high-*T* limit of BPSZ deformation [*Ji and Martignole*, 1994; *Vollbrecht et al.*, 2006]. Similarly, core-and-mantle structures in plagioclase indicate deformation at or above 500–550°C [e.g., *Pryer*, 1993]. There are potential indicators of feldspar SGR, which would imply even higher-*T* deformation, but this texture could also suggest microcracking [*Tullis and Yund*, 1987].

Minimum deformation temperatures are constrained by quartz opening angles to <400°C in the center of the shear zone (Figure 9). However, there is no petrographic evidence for quartz deformation in the corresponding BLG recrystallization regime, as would be expected for this temperature. One possible explanation is that the presence of water in quartz at the 0.1 weight percent level can depress the minimum temperatures required for SGR or GBM textural development by up to 100°C [*Hirth and Tullis*, 1992; *Post et al.*, 1996; *Morgan and Law*, 2004]. Though quartz shows no brittle deformation, the onset of which occurs below ~300°C [e.g., *Stipp et al.*, 2002], fluid-present deformation could have allowed strain to be accommodated to lower temperatures than the quartz fabrics alone would suggest. Overall, the textural data suggest that the shear zone and its wall rocks were deformed over a temperature interval of ~600–350°C.

8.2.2. Quartz Slip Systems Support a Thermal Gradient From Footwall to Hanging Wall During the Early Stages of Shear Zone Activity

The quartz-rich sections of the footwall record mixed basal, rhomb, and prism < a > slip, but the symmetric single girdles in the hanging wall indicate rhomb to prism < a > slip with almost no basal < a > slip (Figure 8). This change indicates the activity of lower-*T* deformation at the base of the shear zone transitioning to higher-*T* quartz slip systems upsection [e.g., *Kurz et al.*, 2002]. Such changes occur when the critically resolved shear stress (CRSS) required for prism and rhomb < a > slip decreases below the CRSS required for basal < a > slip [*Ralser et al.*, 1991] and can be caused by factors other than temperature [*Toy et al.*, 2008]. However, the hanging wall sample that preserves the highest-*T* quartz microstructures (10JG191-1: GBM only) and metamorphic temperature (682 ± 34°C) also preserves the strongest single-girdle fabric, supporting the interpretation of a thermal gradient. The fact that hotter temperatures are recorded by both metamorphic and microstructural data sets strengthens our interpretation that the hanging wall was at least initially hotter than the footwall during BPSZ activity.

An alternative explanation for the slip system changes is that increases in noncoaxial strain intensity from footwall to hanging wall could have also caused a progressive change from basal < a > slip to rhomb/prism < a > slip [e.g., *Schmid and Casey*, 1986]. However, we consider this interpretation less robust, particularly because the symmetric single girdles and coaxial microstructures in hanging wall rocks could not have formed during predominantly simple shear, and rather implicate a *decreasing* component of noncoaxial strain upsection. Furthermore, various experimental [e.g., *Heilbronner and Tullis*, 2006] and natural data [e.g., *Toy et al.*, 2008] have shown that single-girdle *c*-axis distributions formed under increasing noncoaxial strain will be progressively rotated toward the fabric attractor in the shear direction, which is not observed here (Figure 8). Therefore, we favor the interpretation of a thermal gradient from footwall to hanging wall.

The preservation of a thermal gradient in the higher-*T* metamorphic and quartz slip system data, but not in the lower-*T* quartz *c*-axis data (section 8.2.3, below), strongly implies that the gradient initiated in the early stages of shear zone activity at elevated temperatures (>550°C) but was later overprinted. This gradient developed as the footwall was reburied after partial exhumation at 436 ± 4 Ma [*Mulcahy et al.*, 2011]. However, it must have existed prior to final Ar closure in hanging wall hornblende at 405.6 ± 1.7 Ma (sample 10JG191-2), because footwall mineral growth that resulted from overthrusting of the hotter hanging wall records temperatures (620 ± 16°C) that exceed the Ar closure temperature in hornblende (~550°C). These ages are only broad constraints; because inverted thermal gradients along shear zones are transient features [e.g., *England and Molnar*, 1993], the preservation of such a gradient here suggests that it developed only shortly before ~405 Ma.

8.2.3. Quartz *C*-Axis Opening Angles: Potential Record of Progressive Strain Localization to the Center of the BPSZ?

The quartz opening angles and other microstructural observations suggest that retrograde BPSZ activity overprints the thermal gradient recorded by quartz slip systems, resulting in a transition from preserved higher-*T* deformation at the edges of the shear zone and in the surrounding wall rocks (~550–600°C), to lower-*T* deformation in the core of the shear zone (~350–400°C). These data are especially pronounced for the lower half of the shear zone, where opening angles progressively close from the base (555 ± 50°C) to the center of the shear zone (375–470 ± 50°C) (Figure 9). High-temperature deformed quartz with partial annealing at the base of the BPSZ suggest that all rocks were strained at higher *T*, but that continued retrograde deformation in the center of the shear zone produced a lower-*T* overprint while the edges recovered. This recovery would not be expected to have a strong effect on quartz LPOs [e.g., *Heilbronner and Tullis*, 2002], such that each part of the shear zone records its last deformation temperature and therefore the localization event. The footwall outside of the shear zone avoided significant deformation associated with the BPSZ, as indicated by annealed quartz (Figure 7b) and postkinematic metamorphic mineral growth (Figures 6a and 6b), though the qualitative increase in footwall fabric intensity observed in proximity to the shear zone (c.f. sections 3.2, 4.2.1, and 5.2.1) suggests that it was at least somewhat strained during BPSZ activity.

A similar story holds in the upper part of the shear zone and hanging wall, though a lack of opening angles complicates the interpretation. Higher-*T* (>500°C) deformation fabrics preserved in the hanging wall orthogneiss give way to lower-*T* (450–350°C) textures in the upper part of the shear zone, with the lowest-*T* sample in the core showing unrecovered quartz fabrics and an opening angle temperature of 343 ± 50°C (Figure 9b). Annealed fabrics at the upper edge of the shear zone also suggest progressive strain localization with falling temperature. This interpretation would benefit from additional opening angle measurements in the upper part of the shear zone and hanging wall. We suggest that the lack of opening angles and the persistence of single-girdle fabrics may be a function of high strains that "locked in" the quartz slip systems at high *T*, suppressing the activity of basal < a > slip as the rocks were exhumed to lower temperatures [cf. *Toy et al.*, 2008].

Alternative interpretations of the *c*-axis opening angles are possible. In particular, decreases in opening angle (and thus apparent deformation temperature) can occur with increases in strain rate at constant temperature [e.g., *Tullis et al.*, 1973; *Morgan and Law*, 2004], and the transition from GBM to SGR quartz microstructures is promoted at both lower temperatures and higher strain rates [*Hirth and Tullis*, 1992]. Therefore, rather than decreasing deformation temperature, the opening angles may be recording an increase in strain rate from the edge to the center of the shear zone. This interpretation would also support strain localization within the shear zone through time, and our thermochronologic evidence for rapid cooling of the shear zone suggests it was most likely accompanied by a decrease in temperature. While this scenario complicates the correlation between *c*-axis opening angle and *absolute* deformation temperature, the same fundamental conclusion stands. Therefore, we interpret the variation in quartz *c*-axis opening angles as recording late strain localization from the edges to the core of the shear zone.

8.2.4. Summary of BPSZ Deformation and Implications for Strain Localization

The microstructural and quartz *c*-axis data characterize the BPSZ as a high-strain ductile shear zone that began top-to-the-west activity at elevated metamorphic temperatures (>600°C). It was initially characterized by an inverted thermal gradient and more distributed strain that was accompanied by metamorphic mineral growth and Ar isotopic re-equilibration in the footwall, but strain progressively localized to the center of the shear zone as it continued to deform to ~350°C. This localization was best preserved by the metapelitic footwall and base of the shear zone, in which deformation fully localized to the core of the shear zone. Textural observations suggest that the hanging wall orthogneiss experienced similar strain localization, though the absence of quartz *c*-axis opening angles complicates the interpretation.

Our thermochronologic and textural evidence for rapid exhumation implicates cooling as the principal driver of strain localization along the BPSZ, such that the zone of active deformation in the shear zone narrowed as temperature fell and strain rates increased, while the rocks at the edge of the shear zone recovered. This is consistent with evidence from other field studies showing that exhumed lower-crustal high-strain zones are often overprinted by narrower structures at shallower depths [e.g., *Simpson et al.*, 2001; *Beacom et al.*, 2001], and with considerations of the effect of temperature on rock strength in the ductile regime [e.g., *Burgmann and Dresen*, 2008]. However, this localization was initiated and assisted by numerous other processes active over a range of temperatures. For example, the lithologic transition between metapelite and orthogneiss is a

significant rheologic (i.e., strength) contrast. The presence of a major shear zone along the contact indicates that such contrasts were effective at localizing strain in the Pie de Palo even at the most elevated deformation temperatures experienced by the BPSZ. Once the shear zone initiated, dynamic recrystallization and grain size reduction helped to maintain it as a stable low-viscosity zone; the effective viscosity contrast between the shear zone and its adjacent rocks was maintained and may even have been enhanced upon cooling, as rocks adjacent to the shear zone strengthened. We also suggest that fluid flow, which was probably at least partly responsible for the metamorphic mineral growth and Ar isotopic resetting in the footwall, served to weaken the shear zone relative to its wall rocks. Therefore, though we suggest that falling temperatures were the root cause of strain localization in the BPSZ, we emphasize that the specific mechanisms and factors that localized strain were active over a broad thermal range.

A precise assessment of the time scale over which this localization occurred is severely limited by our age and temperature uncertainties. The deformation temperatures recorded by rocks at the edge of the shear zone range from ~550 to 500°C, whereas those in the center of the shear zone are as low as 350°C. Therefore, the $^{40}Ar/^{39}Ar$ ages from hanging wall hornblende (405.6 ± 1.7 Ma) and shear zone muscovite (402 ± 4 Ma), with closure temperatures ~550–500°C and ~425–350°C, show that the localization occurred over a $<$10 Myr interval.

8.3. Tectonic Setting of BPSZ Deformation at ~400 Ma

The early Devonian BPSZ is likely one of a series of shear zones with similar timing in the Pie de Palo, but further research is needed to determine their location and extent. $^{40}Ar/^{39}Ar$ muscovite cooling ages from the Pie de Palo range from ~440–394 Ma [*Ramos et al.*, 1998; *Mulcahy et al.*, 2011; this study] (Figure 2b), but the tectonic significance of this age range is not well understood. Samples with approximately coeval hornblende and muscovite cooling ages are from high-strain zones [*Mulcahy et al.*, 2011; this study] and are interpreted to indicate rapid cooling at the end of a high-strain event. Other white mica ages without coeval hornblende ages are also proximal to major shear zones, including the Las Pirquitas Thrust on the west side of the Pie de Palo, but two such samples record quite different cooling ages, 395.7 ± 0.2 Ma [*Ramos et al.*, 1998] and 417 ± 2 Ma [*Mulcahy et al.*, 2011]. Thus, the number and timing of discrete shear events on regional structures in the Pie de Palo remains to be determined.

However, the early Devonian deformation documented in this study coincides with numerous tectonic events preserved elsewhere along the mid-Paleozoic Gondwana margin, suggesting considerable crustal reorganization during the later stages of the Famatinian collisional system. In particular, several coeval ductile shear zones are well-documented to the east of the Pie de Palo. High-grade metamorphic rocks in the Loma de Las Chacras, located immediately west of the Valle Fértil lineament (Figure 1), record extension, exhumation, and decompression by 400 Ma [*Cain*, 2005; *Mulcahy et al.*, 2014], following two phases of migmatization. The initial, high-*T*/high-*P* migmatite event in Las Chacras peaked ~470–460 Ma and was associated with widespread lower-crustal melting, yet the rocks were not significantly exhumed and instead experienced slow isobaric cooling for tens of Myr [*Mulcahy et al.*, 2014]. These migmatites were reburied and experienced a second phase of lower-crustal migmatization at 411–407 Ma, followed by rapid exhumation from 405–400 Ma [*Mulcahy et al.*, 2014].

Activity along the BPSZ is also coincident with major transpressional structures in the Eastern Sierras Pampeanas such as the Tinogasta-Pituil-Antinaco (TIPA) Shear Zone [e.g., *Hockenreiner et al.*, 2003] (Figure 1, Sierras de Velasco and de Fiambalá), though the timing of activity along such structures is complicated by elevated analytical uncertainties. The age of these shear zones overlaps with intrusive igneous rocks in the region that were emplaced from 400 to 340 Ma [*Sims et al.*, 1998; *van Gosen and Prozzi*, 1998; *Steenken et al.*, 2008] (Figure 1, Sierra de San Luis). Rocks to the west of the Pie de Palo document the development of the Punta Negra foreland basin from 410 to 380 Ma [e.g., *Astini et al.*, 1995].

Previous workers have attributed this regional Devonian tectonism to the approach and collision of the Chilenia terrane, which would have occurred after the final docking of the Precordillera to Gondwana [e.g., *Ramos et al.*, 1998]. However, peak metamorphic conditions associated with the Chilenian collision occurred around 390–385 Ma [*Davis et al.*, 1999; *Gerbi et al.*, 2002; *Willner et al.*, 2011], or ~10 Ma after the shortening documented here. Therefore, we suggest that the BPSZ and other late structures in the Pie de Palo do not record the Chilenia collision *sensu stricto*, but rather shortening and exhumation associated with the reestablishment of a convergent plate margin [cf. *Mulcahy et al.*, 2014]. Once the Chilenia microplate collided,

deformation and magmatism were partitioned away from the Pie de Palo and the Famatinian margin, which experienced no significant Paleozoic deformation after ~400 Ma. The absence of ductile structures in the Pie de Palo after ~400 Ma reinforces our interpretation that final exhumation of all units to the middle crust had occurred by this time.

8.4. Regional-Scale Strain Localization

The comparison of BPSZ structural style and timing with other regional structures elucidates the time-dependent rheological character of ductile shear zones in the Pie de Palo and similar rocks to the east (Loma de Las Chacras). The penetrative Ordovician metamorphism and nappe-style tectonics concentrated at 470–460 Ma [*Casquet et al.*, 2001; *Vujovich et al.*, 2004; *Mulcahy et al.*, 2011; *van Staal et al.*, 2011] are generally preserved in most crustal units, with later structures overprinting this widespread ductile deformation. Kilometer-scale mylonitic shear zones, such as the Duraznos and Higueritas shear zones of *Mulcahy et al.* [2011], record ductile deformation associated with synconvergent exhumation and extension at 440–435 Ma. By 405–395 Ma, deformation was concentrated along the narrow, mylonitic to ultramylonitic structures such as the Don Juan/Flechal shear zone in the Loma de Las Chacras [*Cain*, 2005; *Mulcahy*, 2009; *Mulcahy et al.*, 2014] and the Bajo Pequeño shear zone in the Pie de Palo (this work). In both regions, final reburial and subsequent exhumation of units happened relatively quickly compared to the previous slow cooling from peak Ordovician metamorphism. Additional cooling ages from the Pie de Palo may also document a phase of deformation from 417 to 415 Ma [*Mulcahy et al.*, 2011].

The specific styles of activity and zones of deformation associated with each time period suggest a pattern of regional strain localization in the Famatinian forearc, from penetrative metamorphism and deformation to focused activity along hectometer- and meter-scale structures. This progressive localization was accommodated by short pulses of deformation (5–10 Ma) punctuated by longer periods of quiescence (15–30 Ma). It remains to be seen, however, if these quiescent periods occurred while tectonic deformation was partitioned elsewhere along the Paleozoic Gondwanan margin, or if they represent lulls in the accommodation of tectonic strain; continued regional-scale analyses should help clarify this question.

Regardless of its expression, the causes of this regional-scale strain localization are most likely due to broad thermal changes in the lower crust, likely associated with long-term cooling after major arc volcanism ceased at ~465 Ma [*Dahlquist et al.*, 2008; *Ducea et al.*, 2010]. Transient factors (fluids, melt, etc.) may have played a part, but these factors would have been activated locally along individual shear zones in response to or in concert with the temperature variations, as seen in the BPSZ. In their structural analysis of the westernmost part of the Pie de Palo, *van Staal et al.* [2011] noted a similar localizing trend from homogenously-distributed flow (their F_2) associated with peak metamorphism (~465 Ma) to deformation along localized, retrograde structures; the authors ascribed these changes to "an evolving thermal regime… in the subduction channel" [*van Staal et al.*, 2011]. Our results are broadly consistent with their conclusions; however, this study shows that localization continued ~60–70 Ma after the initial collision began along the western margin of Gondwana, and thus other factors must have contributed to changes in strain localization. One potential influence is the progressive shortening and exhumation events documented by rocks in the Pie de Palo [*Mulcahy et al.*, 2011; this work], which would have enhanced the localization of strain in multiple ways: each shortening event resulted in the development of weak zones with drastically-reduced viscosity, while rapid cooling and exhumation limited recovery from high strain and ensured that shear zones remained as "permanent" weaknesses as adjacent rocks strengthened. Inherent lithological and rheological heterogeneities in the section must have also contributed to regional strain localization, as ductile shear zones in the Pie de Palo and Loma de las Chacras are focused along major contacts. Other important factors could include changes in plate boundary dynamics or plate velocities [*Mulcahy et al.,* 2014] manifested as changes in shear zone widths [*Platt and Behr*, 2011a], or changes in the presence or absence of partial melt along major shear zones in the Pie de Palo and other similar rocks [e.g., *Mulcahy*, 2009; *Mulcahy et al.*, 2011].

9. Conclusions

Integrated field and analytical data from the lower-crustal, top-to-the-west Bajo Pequeño Shear Zone indicate a renewed phase of burial and exhumation during the waning stages of a collisional orogeny. The lithotectonic packages separated by the BPSZ record discrete detrital, metamorphic, deformational, and thermal histories prior to their juxtaposition in the early Devonian (405–400 Ma). Along with data from *Mulcahy et al.* [2011], we show that the footwall Duraznos Complex was metamorphosed at lower-crustal conditions at 469 ± 21 Ma,

partially exhumed at 440–435 Ma, and reburied prior to 405.6 ± 1.7 Ma. In contrast, the hanging wall Bajo Pequeño Gneiss was metamorphosed in the lower crust at 472 ± 13 Ma but was not significantly exhumed prior to 405.6 ± 1.7 Ma, suggesting that the footwall and hanging wall were at crustal levels up to 10 km apart prior to activity along the BPSZ.

Metamorphic, microstructural, and $^{40}Ar/^{39}Ar$ thermochronology data indicate that the shear zone began deforming at >600°C after 436 ± 4 Ma, and was initially characterized by more distributed deformation and a thermal gradient from footwall to hanging wall, resulting in footwall metamorphic mineral growth and argon isotopic reequilibration in the presence of a fluid. Continuing deformation under decreasing temperatures and increasing strain rates forced strain to progressively localize to the center of the shear zone, while the edges of the shear zone recovered. This localization occurred over a short interval (<10 Myr) as the BPSZ cooled through hornblende Ar closure (550–500°C) at 405.6 ± 1.7 Ma and ceased deforming at temperatures near muscovite Ar closure (425–350°C) at 402 ± 4 Ma. The coincident hornblende and muscovite ages indicate fast cooling during exhumation to the middle crust and further indicate that cooling was the dominant driver for strain localization along the BPSZ, though other factors were instrumental in allowing strain to localize.

The timing of shortening and exhumation along the BPSZ is synchronous with motion along other regional structures, as well as renewed igneous activity and foreland basin development, suggesting a major period of lower-crustal reorganization associated with the reestablishment of a convergent plate boundary prior to the collision of the Chilenia microplate. Furthermore, a comparison of ductile structures across the Pie de Palo and other similar rocks (Loma de Las Chacras) suggests that the timing of shear zone activity correlates with structural style and shear zone thickness, resulting in a pattern of regional strain localization over a long time-scale (60–70 Myr), in contrast to the <10 Myr strain localization along the BPSZ. We suggest that thermal changes in the crust are also responsible for this localization, though it was probably enhanced by influences active on larger spatial and time scales, such as progressive shortening/exhumation events, lithological and rheological heterogeneities, changes in plate boundary dynamics, or changes in the presence or absence of partial melt.

Acknowledgments

We would like to thank M. Naipauer for assistance in the field and H.W. Day and M.I. Billen for providing helpful comments and critical insight on an early version of the manuscript. K. Barton and the Department of Plant Biology, Carnegie Institution of Washington, are thanked for access to the SEM for EBSD analyses. D. Mainprice is thanked for sharing his software for plotting pole figures. This work was funded by two UC-Davis Durrell grants and a Geological Society of America graduate student research grant to J.M. Garber. We are grateful to K. Klepeis and C. Casquet for thorough reviews that strengthened the manuscript. All data presented in this paper are either included as supporting information or are available for free upon request from the corresponding author.

References

Allmendinger, R. W., D. Figueroa, D. Snyder, J. Beer, C. Mpodozis, and B. L. Isacks (1990), Foreland shortening and crustal balancing in the Andes and 30°S latitude, *Tectonics*, *9*(4), 789–809, doi:10.1029/TC009i004p00789.

Alvarado, P., S. Beck, G. Zandt, M. Araujo, and E. Triep (2005), Crustal deformation in the south-central Andes backarc terranes as viewed from regional broad-band seismic waveform modeling, *Geophysics J. Int.*, *163*, 580–598.

Anders, E., and N. Grevesse (1989), Abundances of the elements; meteoritic and solar, *Geochim. Cosmochim. Acta*, *53*(1), 197–214.

Astini, R. A., J. L. Benedetto, and N. E. Vaccari (1995), The early Paleozoic evolution of the Argentine Precordillera as a Laurentian rifted, drifted, and collided terrane: A geodynamic model, *Geol. Soc. Am. Bull.*, *107*(3), 253–273.

Austin, L. J., S. M. Roeske, J. M. Garber, J. Winpenny, and Q. Yin (2011), Detrital zircon geochronology of lower to mid-crustal rocks associated with a microplate-continent collision, NW Argentina, Abstract T51A-2317 presented at 2011 Fall Meeting, AGU, San Francisco, Calif., 5–9 Dec.

Baldo, E., C. Casquet, R. J. Pankhurst, C. Galindo, C. W. Rapela, C. M. Fanning, J. Dahlquist, and J. Murra (2006), Neoproterozoic A-type magmatism in the Western Sierras Pampeanas (Argentina): Evidence for Rodinia break-up along a proto-Iapetus rift?, *Terra Nova*, *18*(6), 388–394, doi:10.1111/j.1365-3121.2006.00703.x.

Beacom, L. E., R. E. Holdsworth, K. J. W. McCaffrey, and T. B. Anderson (2001), A quantitative study of the influence of pre-existing compositional and fabric heterogeneities upon fracture-zone development during basement reactivation, in *The Nature and Tectonic Significance of Fault Zone Weakening*, edited by R. E. Holdsworth et al., *Geol. Soc. London Spec. Publ.*, *186*, 195–211.

Bjørnerud, M., and H. Austrheim (2002), Comment on: "Evidence for shear heating, Musgrave Block, central Australia" by A. Camacho, I. McDonald, R. Armstrong, and J. Braun, *J. Struct. Geol.*, *24*, 1537–1538.

Black, L. P., et al. (2004), Improved $^{206}Pb/^{238}U$ microprobe geochronology by the monitoring of a trace-element-related matrix effect; SHRIMP, ID-TIMS, ELA-ICP-MS and oxygen isotope documentation for a series of zircon standards, *Chem. Geol.*, *205*, 115–140.

Burgmann, R., and G. Dresen (2008), Rheology of the lower crust and upper mantle: Evidence from rock mechanics, geodesy, and field observations, *Annu. Rev. Earth Planet. Sci.*, *36*, 531–567.

Cain, J. C. (2005), Characterization of the Don Juan Shear Zone: Devonian extension in the Western Sierras Pampeanas, Provincia San Juan, Argentina, MS thesis, Dept. of Geology, Univ. of Calif., Davis.

Camacho, A. (2002), Reply to Comment on: "Evidence for shear heating, Musgrave Block, central Australia" by A. Camacho, I. McDougall, R. Armstrong, and J. Braun, *J. Struct. Geol.*, *24*, 1539–1540.

Camacho, A., I. McDougall, R. Armstrong, and J. Braun (2001), Evidence for shear heating, Musgrave Block, central Australia, *J. Struct. Geol.*, *23*, 1007–1013.

Casquet, C., E. Baldo, R. J. Pankhurst, C. W. Rapela, C. Galindo, C. M. Fanning, and J. Saavedra (2001), Involvement of the Argentine Precordillera terrane in the Famatinian mobile belt: U-Pb SHRIMP and metamorphic evidence from the Sierra de Pie de Palo, *Geology*, *29*(8), 703–706, doi:10.1130/0091-7613(2001)029<0703:IOTAPT>2.0.CO;2.

Casquet, C., C. W. Rapela, R. J. Pankhurst, E. G. Baldo, C. Galindo, C. M. Fanning, J. A. Dahlquist, and J. Saavedra (2012), A history of Proterozoic terranes in southern South America: From Rodinia to Gondwana, *Geosci. Front.*, *3*(2), 137–145, doi:10.1016/j.gsf.2011.11.004.

Dahl, P. S. (1996), The effects of composition on retentivity of argon and oxygen in hornblende and related amphiboles: A field-tested empirical model, *Geochim. Cosmochim. Acta*, *60*(19), 3687–3700.

Dahlquist, J. A., R. J. Pankhurst, C. W. Rapela, C. Galindo, P. Alasino, C. M. Fanning, J. Saavedra, and E. Baldo (2008), New SHRIMP U-Pb data from the Famatina Complex: Constraining early-mid Ordovician Famatinian magmatism in the Sierras Pampeanas, Argentina, *Geologica Acta*, *6*(4), 319–333.

Davis, J. S., S. M. Roeske, W. C. McClelland, and L. W. Snee (1999), Closing the ocean between the Precordillera terrane and Chilenia: Early Devonian ophiolite emplacement and deformation in the SW Precordillera, in *Laurentia-Gondwana Connections Before Pangea*, edited by V. A. Ramos and J. D. Keppie, *Geol. Soc. Am. Spec. Pap.*, *336*, 115–138.

Ducea, M. N., J. E. Otamendi, G. Bergantz, K. M. Stair, V. A. Valencia, and G. E. Gehrels (2010), Timing constraints on building an intermediate plutonic arc crustal section: U-Pb zircon geochronology of the Sierra Valle Fértil-La Huerta, Famatinian arc, Argentina, *Tectonics*, *29*(4), doi:10.1029/2009TC002615.

Dunlap, W. J. (1997), Neocrystallization or cooling? $^{40}Ar/^{39}Ar$ age of white micas from low-grade mylonites, *Chem. Geol.*, *143*, 181–205.

England, P., and P. Molnar (1993), The interpretation of inverted metamorphic isograds using simple physical calculations, *Tectonics*, *12*(1), 145–158, doi:10.1029/92TC00850.

Faleiros, F. M., G. A. da Cruz Campanha, R. M. da Silbeira Bello, and K. Fuzikawa (2010), Quartz recrystallization regimes, c-axis texture transitions and fluid inclusion reequilibration in a prograde greenschist to amphibolite facies mylonite zone (Ribeira Shear Zone, SE Brazil), *Tectonophysics*, *485*, 193–214, doi:10.1016/j.tecto.2009.12.014.

Galindo, C., C. Casquet, C. Rapela, R. J. Pankhurst, E. Baldo, and J. Saavedra (2004), Sr, C, and O isotope geochemistry and stratigraphy of Precambrian and lower Paleozoic carbonate sequences from the Western Sierras Pampeanas of Argentina: Tectonic implications, *Precambrian Res.*, *131*, 55–71.

Gerbi, C., S. M. Roeske, and J. S. Davis (2002), Geology and structural history of the southwest Precordillera margin, northern Mendoza Province, Argentina, *J. South Amer. Earth Sci.*, *14*, 821–835.

Gimenez, M. E., M. P. Martinez, and A. Introcaso (2000), A crustal model based mainly on gravity data in the area between the Bermejo Basin and the Sierras de Valle Fértil, Argentina, *J. South Amer. Earth Sci.*, *13*, 275–286.

Harrison, T. M., J. Célérier, A. B. Aikman, J. Hermann, and M. T. Heizler (2009), Diffusion of ^{40}Ar in muscovite, *Geochim. Cosmochim. Acta*, *73*, 1039–1051.

Heilbronner, R., and J. Tullis (2002), The effect of static annealing on microstructure and crystallographic preferred orientations of quartzites experimentally deformed in axial compression and shear, in *Deformation Mechanisms, Rheology and Tectonics: Current Status and Future Perspectives*, edited by S. de Meer et al., *Geol. Soc. London Spec. Publ.*, *200*, 191–218.

Heilbronner, R., and J. Tullis (2006), Evolution of c-axis pole figures and grain size during dynamic recrystallization: Results from experimentally-sheared quartzite, *J. Geophys. Res.*, *111*, B10202, doi:10.1029/2005JB004194.

Hirth, G., and J. Tullis (1992), Dislocation creep regimes in quartz aggregates, *J. Struct. Geol.*, *14*(2), 145–159.

Hockenreiner, M., F. Söllner, and H. Miller (2003), Dating the TIPA shear zone: An early Devonian terrane boundary between the Famatinian and Pampean systems (NW Argentina), *J. South Amer. Earth Sci.*, *16*, 45–66.

Holland, T. J. B., and R. Powell (1998), An internally consistent thermodynamic dataset for phases of petrologic interest, *J. Metamorph. Geol.*, *16*, 309–343.

Ji, S., and J. Martignole (1994), Ductility of garnet as an indicator of extremely high temperature deformation, *J. Struct. Geol.*, *16*(7), 985–996.

Kidder, S., and M. N. Ducea (2006), High temperatures and inverted metamorphism in the schist of Sierra de Salina, California, *Earth Planet. Sci. Lett.*, *241*, 422–437.

Korotev, R. L. (1996), A self-consistent compilation of elemental concentration data for 93 geochemical reference samples, *Geostand. Newsl.*, *20*, 217–245.

Kretz, R. (1983), Symbols for rock-forming minerals, *Am. Mineral.*, *68*, 277–279.

Kruhl, J. H. (1998), Reply to Comment on "Prism- and basal-plane parallel subgrain boundaries in quartz; a microstructural geothermobarometer" by T. Okudaira, T. Takeshita, and M. Toriumi, *J. Metamorph. Geol.*, *16*, 142–146.

Kuhn, A., J. Glodny, K. Iden, and H. Austrheim (2000), Retention of Precambrian Rb/Sr phlogopite ages through Caledonian eclogite facies metamorphism, Bergen Arc Complex, W-Norway, *Lithos*, *51*, 305–330.

Kurz, W., H. Fritz, V. Tenczer, and W. Unzog (2002), Tectonometamorphic evolution of the Koralm Complex (Eastern Alps); constraints from microstructures and textures of the "Plattengneis" shear zone, *J. Struct. Geol.*, *24*, 1957–1970.

Law, R. D., M. P. Searle, and R. L. Simpson (2004), Strain, deformation temperatures and vorticity of low at the top of the Greater Himalayan Slab, Everest Massif, Tibet, *J. Geol. Soc. London*, *161*, 305–320.

Lister, G. S. (1977), Discussion: Crossed girdle c-axis fabrics in quartzites plastically deformed by plane strain and progressive simple shear, *Tectonophysics*, *39*, 51–54, doi:10.1016/0040-1951(77)90087-7.

Locock, A. J. (2008), An Excel spreadsheet to recast analyses of garnet into end-member components, and a synopsis of the crystal chemistry of natural silicate garnets, *Comput. Geosci.*, *34*, 1769–1780.

Ludwig, K. R. (2001), *SQUID 1.02, A User's Manual*, vol. 2, Berkeley Geochronology Centre Special Publication, Berkeley, Calif.

Ludwig, K. R. (2003), *Isoplot/Ex Version 3.0: A Geochronological Toolkit for Microsoft Excel*, vol. 4, Berkeley Geochronology Center Special Publication, Berkeley, Calif.

Maitland, T., and S. Sitzman (2007), Electron backscatter diffraction (EBSD) technique and materials characterization examples, in *Scanning Microscopy for Nanotechnology: Techniques and Applications*, edited by W. Zhou and Z. L. Wang, pp. 41–75, Springer-Verlag, Berlin, Germany.

Mattinson, C. G., J. L. Wooden, J. X. Zhang, and D. K. Bird (2009), Paragneiss zircon geochronology and trace element geochemistry, North Qaidam HP/UHP terrane, western China, *J. Asian Earth Sci.*, *35*, 298–309.

Mazdab, F. K., and J. L. Wooden (2006), Trace element analysis in zircon by ion microprobe (SHRIMP-RG); technique and applications, *Geochim. Cosmochim. Acta*, *70*(18S), doi:10.1016/j.gca.2006.06.817.

McDonough, M. R., V. A. Ramos, C. E. Isachsen, S. A. Bowring, and G. I. Vujovich (1993), Edades preliminares de circones del basamento de la Sierra de Pie de Palo, Sierras Pampeanas occidentales de San Juan: Sus implicancias para el supercontinente Proterozoico de Rodinia, in *XIII Congreso Geológico Argentino y II Congreso de Exploración de Hidrocarburos*, vol. 3, pp. 340–342, Argentine Geol. Congr, Buenos Aires.

Morgan, S. S., and R. D. Law (2004), Unusual transition in quartzite dislocation creep regimes and crystal slip systems in the aureole of the Eureka Valley–Joshua Flat–Beer Creek pluton, California: A case for anhydrous conditions created by decarbonation reactions, *Tectonophysics*, *384*, 209–231, doi:10.1016/j.tecto.2004.03.016.

Mulcahy, S. R. (2009), Structural and metamorphic evolution of a Paleozoic middle- to lower-crustal section in the Western Sierras Pampeanas of northwest Argentina, PhD dissertation, Dept. of Geology, Univ. of Calif., Davis.

Mulcahy, S. R., S. M. Roeske, W. C. McClelland, S. Nomade, and P. R. Renne (2007), Cambrian initiation of the Las Pirquitas thrust of the Western Sierras Pampeanas, Argentina: Implications for the tectonic evolution of the proto-Andean margin of South America, *Geology*, *35*, 443–446.

Mulcahy, S. R., S. M. Roeske, W. C. McClelland, F. Jourdan, A. Iriondo, P. R. Renne, J. D. Vervoort, and G. I. Vujovich (2011), Structural evolution of a composite middle to lower crustal section: The Sierra de Pie de Palo, northwest Argentina, *Tectonics*, *30*, doi:10.1029/2009TC002656.

Mulcahy, S. R., S. M. Roeske, W. C. McClelland, J. R. Ellis, F. Jourdan, P. R. Renne, J. D. Vervoort, and G. I. Vujovich (2014), Multiple migmatite events and cooling from granulite facies metamorphism within the Famatina arc margin of northwest Argentina, *Tectonics*, *33*, 1–25, doi:10.1002/2013TC003398.

Okudaira, T., T. Takeshita, I. Hara, and J. Ando (1995), A new estimate of the conditions for transition from basal < a > to prism [c] slip in naturally deformed quartz, *Tectonophysics*, *250*, 31–46, doi:10.1016/0040-1951(95)00039-4.

Passchier, C. W., and R. A. J. Trouw (2005), *Microtectonics*, 2nd ed., Springer-Verlag, Berlin, Germany.

Pidgeon, R. T., D. Furfaro, A. K. Kennedy, A. A. Nemchin, and W. van Bronswjk (1994), Calibration of zircon stands for the Curtin SHRIMP II, Abstracts of the 8th International Conference on Geochronology, Cosmochronology, and Isotope Geology, Berkeley, USA, U.S. Geol. Survey Circular, 1107, 251.

Platt, J. P., and W. M. Behr (2011a), Lithospheric shear zones as constant stress experiments, *Geology*, *39*(2), 127–130.

Platt, J. P., and W. M. Behr (2011b), Grainsize evolution in ductile shear zones: Implications for strain localization and the strength of the lithosphere, *J. Struct. Geol.*, *33*, 537–550.

Post, A. D., J. Tullis, and R. A. Yund (1996), Effects of chemical environment on dislocation creep of quartzite, *J. Geophys. Res.*, *101*(B10), 22,143–22,155, doi:10.1029/96JB01926.

Powell, R., and T. Holland (1994), Optimal geothermometry and geobarometry, *Am. Mineral.*, *79*, 120–133.

Prior, D. J., et al. (1999), The application of electron backscatter diffraction and orientation contrast imaging in the SEM to textural problems in rocks, *Am. Mineral.*, *84*, 1741–1759.

Pryer, L. L. (1993), Microstructures in feldspars from a major crustal thrust zone: The Grenville Front, Ontario, Canada, *J. Struct. Geol.*, *15*(1), 21–36.

Ralser, S., B. E. Hobbs, and A. Ord (1991), Experimental deformation of a quartz mylonite, *J. Struct. Geol.*, *13*(7), 837–850.

Ramos, V. A., and G. I. Vujovich (2000), Hoja geológica San Juan, escala 1:250000, Servicio Geológico Minero Argentino, Boletín, Buenos Aires, Argentina.

Ramos, V. A., R. D. Dallmeyer, and G. I. Vujovich (1998), Time constraints on the early Paleozoic docking of the Precordillera, central Argentina, in *The Proto-Andean Margin of Gondwana*, edited by R. J. Pankhurst and C. W. Rapela, *Geol. Soc. London Spec. Publ.*, *142*, 143–158.

Ramos, V. A., E. O. Cristallini, and D. J. Pérez (2002), The Pampean flat-slab of the central Andes, *J. South Amer. Earth Sci.*, *15*, 59–78.

Rapela, C. W., R. J. Pankhurst, C. Casquet, E. Baldo, C. Galindo, C. M. Fanning, and J. M. Dahlquist (2010), The Western Sierras Pampeanas: Protracted Grenville-age history (1330–1030 Ma) of intra-oceanic arcs, subduction-accretion at continental-edge and AMCG intraplate magmatism, *J. South Amer. Earth Sci.*, *29*, 105–127.

Renne, P. R., C. C. Swisher, A. L. Deino, D. B. Karner, T. L. Owens, and D. J. DePaolo (1998), Intercalibration of standards, absolute ages and uncertainties in $^{40}Ar/^{39}Ar$ dating, *Chem. Geol.*, *145*, 117–152.

Renne, P. R., G. Balco, K. R. Ludwig, R. Mundil, and K. Min (2011), Joint determination of ^{40}K decay constants and $^{40}Ar^*/^{40}K$ for the Fish Canyon sanidine standard, and improved accuracy for $^{40}Ar/^{39}Ar$ geochronology, *Geochim. Cosmochim. Acta*, *75*(17), 5097–5100.

Rutter, E. H., R. E. Holdsworth, and R. J. Knipe (2001), The nature and tectonic significance of fault-zone weakening: An introduction, in *The Nature and Tectonic Significance of Fault Zone Weakening*, edited by R. E. Holdsworth et al., *Geol. Soc. London Spec. Publ.*, *186*, 1–11.

Schmid, S., and M. Casey (1986), Complete fabric analysis of some commonly observed quartz c-axis patterns, *Geophysical Monograph*, *36*, 263–286.

Simpson, C., S. J. Whitmeyer, D. G. de Paor, L. P. Gromet, R. Miro, M. A. Krol, and H. Short (2001), Sequential ductile to brittle reactivation of major fault zones along the accretionary margin of Gondwana in Central Argentina, in *The Nature and Tectonic Significance of Fault Zone Weakening*, edited by R. E. Woolworth et al., *Geol. Soc. London Spec. Publ.*, *186*, 233–255.

Sims, J. P., T. R. Ireland, A. Camacho, P. Lyons, P. E. Pieters, R. G. Skirrow, P. G. Stuart-Smith, and R. Miró (1998), U-Pb, Th-Pb, and Ar-Ar geochronology from the southern Sierras Pampeanas, Argentina: Implications for the Palaeozoic tectonic evolution of the western Gondwana margin, in *The Proto-Andean Margin of Gondwana*, edited by R. J. Pankhurst and C. W. Rapela, *Geol. Soc. London Spec. Publ.*, *142*, 259–281.

Stacey, J. S., and J. D. Kramers (1975), Approximation of terrestrial lead isotope evolution by a two-stage model, *Earth Planet. Sci. Lett.*, *26*(2), 207–221.

Steenken, A., S. Siegesmund, K. Wemmer, and M. G. Lopez de Luchi (2008), Time constraints on the Famatinian and Achalian structural evolution of the basement of the Sierra de San Luis (eastern Sierras Pampeanas, Argentina), *J. South Amer. Earth Sci.*, *25*(3), 336–358.

Stipp, M., H. Stünitz, R. Heilbronner, and S. M. Schmid (2002), The eastern Tonale fault zone: A "natural laboratory" for crystal plastic deformation of quartz over a temperature range from 250–700°C, *J. Struct. Geol.*, *24*, 1861–1884.

Takeshita, T. (1996), Estimate of the physical conditions for deformation based on c-axis fabric transitions in naturally deformed quartzite, *J. Geol. Soc. Jpn.*, *102*, 211–222.

Toy, V. G., D. J. Prior, and R. J. Norris (2008), Quartz fabrics in the Alpine Fault mylonites: Influence of pre-existing preferred orientations on fabric development during progressive uplift, *J. Struct. Geol.*, *30*, 602–621.

Tullis, J., and R. A. Yund (1987), Transition from cataclastic flow to dislocation creep of feldspar: Mechanisms and microstructures, *Geology*, *15*, 606–609.

Tullis, J., J. M. Christie, and D. T. Griggs (1973), Microstructures and preferred orientations of experimentally-deformed quartzites, *Geol. Soc. Am. Bull.*, *84*, 297–314.

van Gosen, W., and C. Prozzi (1998), Structural evolution of the Sierra de San Luis (Eastern Sierras Pampeanas, Argentina): Implications for the proto-Andean margin of Gondwana, in *The Proto-Andean Margin of Gondwana*, edited by R. J. Pankhurst and C. W. Rapela, *Geol. Soc. London Spec. Publ.*, *142*, 235–258.

van Staal, C. R., G. I. Vujovich, K. L. Currie, and M. Naipauer (2011), An Alpine-style Ordovician collision complex in the Sierra de Pie de Palo, Argentina: Record of subduction of Cuyania beneath the Famatinian arc, *J. Struct. Geol.*,, *33*, 343–361.

Vernon, R. H., R. W. White, and G. L. Clarke (2008), False metamorphic events inferred from misinterpretation of microstructural evidence and *P-T* data, *J. Metamorph. Geol.*, *26*, 437–449.

Vollbrecht, A., J. Pawlowski, B. Leiss, T. Heinrichs, M. Seidel, and A. Kronz (2006), Ductile deformation of garnet in mylonitic gneisses from the Münchberg Massif (Germany), *Tectonophysics*, *427*, 153–170.

Vujovich, G. I., C. R. van Staal, and W. Davis (2004), Age constraints on the tectonic evolution and provenance of the Pie de Palo complex, Cuyania composite terrane, and the Famatinian orogeny in the Sierra de Pie de Palo, San Juan, Argentina, *Gondwana Res.*, *7*, 1041–1056.

Waters-Tormey, C., and B. Tikoff (2007), Characteristics of a kilometer-scale high strain zone in the lower continental crust: Mt. Hay block, central Australia, *J. Struct. Geol.*, *29*, 562–582.

White, J. C. (2004), Instability and localization of deformation in lower crust granulites, Minas fault zone, Nova Scotia, Canada, in *Flow Processes in Faults and Shear Zones*, edited by G. I. Alsop et al., *Geol. Soc. London Spec. Publ.*, *224*, 25–37.

Williams, I. S. (1998), U-Th-Pb geochronology by ion microprobe, in *Application of Microanalytical Techniques to Understanding Mineralizing Processes*, *Reviews in Economic Geology*, vol. 7, edited by M. A. McKibben et al., pp. 1–35, Society of Economic Geologists, Littleton, Colo.

Williams, M. L., K. E. Karlstrom, G. Dumond, and K. H. Mahan (2009), Perspectives on the architecture of continental crust from integrated field studies of exposed isobaric sections, in *Crustal Cross Sections from the Western North American Cordillera and Elsewhere: Implications for Tectonic and Petrology Processes*, edited by R. B. Miller and A. W. Snoke, *Geol. Soc. Am. Spec. Pap.*, *456*, 219–241.

Willner, A. P., A. Gerdes, H.-J. Massonne, A. Schmidt, M. Sudo, S. N. Thomson, and G. I. Vujovich (2011), The geodynamics of collision of a microplate (Chilenia) in Devonian times deduced by the pressure-temperature-time evolution within part of a collisional belt (Guarguaraz Complex, W-Argentina), *Contrib. Mineral. Petrol.*, *162*, 303–327.

Zapata, T. R. (1998), Crustal structure of the Andean thrust front at 30°S latitude from shallow and deep seismic reflection profiles, Argentina, *J. South Amer. Earth Sci.*, *11*(2), 131–151.